

**The Study of Intravascular Stent Design Parameters to  
Reduce Restenosis Risk by Considering  
A Transient Non-uniform Balloon-Stent Expansion**

*Won-Pil Park*

The Graduate School

Yonsei University

Department of Biomedical Engineering

**The Study of Intravascular Stent Design Parameters to  
Reduce Restenosis Risk by Considering  
A Transient Non-uniform Balloon-Stent Expansion**

A Master's Thesis

Submitted to the Department of Biomedical Engineering

and the Graduate School of Yonsei University

in partial fulfillment of the



requirements for the degree of


Master of Biomedical Engineering


***Won-Pil Park***

June 2008

This certifies that the master's thesis of *Won-Pil Park* is approved.

[Signature]   
Thesis Supervisor: Han Sung Kim 

[Signature]   
Young Ho Kim 

[Signature]   
Dohyoung Lim 

The Graduate School

Yonsei University

June 2008

## ACKNOWLEDGEMENTS

이 연구결과가 나오기까지 대학원 재학기간 동안에 저에게 진취적이고 역동적인 연구를 진행할 수 있게 물심양면으로 도와주시고 지도해주신 김한성 교수님께 깊은 존경과 감사의 뜻을 올립니다. 또한 미흡한 저의 학위논문을 심사해주신 김영호 교수님께도 감사의 말씀을 올립니다. 글로써 모두 다 표현할 수 없다는 것이 안타까울 정도로 대학원 재학기간 동안 큰 형님처럼 여러 면에서 도와주셨던 임도형 교수님께도 감사를 드립니다.

속마음을 좀처럼 내비치지 않는 신비주의 Concept 대곤이형, 어쩌다 보니 무슨 일만 했다 하면 나랑 많이 겹치는 바람에 고생 많이 했었던 승관이형, 앞으로의 명칭이 고박사라는 것이 개인적으로 유감인 창용이형, 의공학계의 All-round Player 태우, 키만 좀 컸으면 여러 여자 (특히 연상) 건드리고 다녔을 영근이, 다 좋은데 눈치가 9 $\mu$  단인 현동이, 의도된 건지 기획된 건지 모르겠지만 콧소리가 인상적인 효선이, 열의에 불타는 불꽃남자 선욱이, 연구실의 영원한 왕고참 창수형, 학번상 동기인데 별로 마주칠 일 없었던 은정이, 나보고 맨날 살찌라고 하면서 자기만 살찌는 성식이형, 얼굴 큰 거 빼놓곤 내가 바라는 이상적 몸매(크고 긴)를 가진 현호형, 학부 때부터 이런 저런 일 같이 많이 하다 보니 연구실 멤버 중에서 가장 정감이 가는 범석이, 모든 대학원 타 연구실의 선·후배님들에게도 감사의 뜻을 전합니다.

그 외에도 이 글에 다 적진 못했지만 제가 기억하고, 저를 기억해주시는 모든 친척, 친구, 관계자 분들께도 감사의 뜻을 전합니다.

남들이 이런 순서로 적다 보니 뒤로 밀리긴 했지만, 그 어느 누구보다도 제가 제일 먼저 감사 드리고 싶은 저의 부모님, 이 못난 녀석도 자식이라고 끝까지 믿어주시고 보살펴주셨기에 지금의 제가 있을 수 있었습니다. 감사합니다. 어릴 땐 많이 때리고 괴롭히더니 나이 먹고 철든 다음부턴 나에게 잘 해주는 우리 형, 나이를 먹을수록 더 무뎡뎡해지는 애교 Free 우리 누나에게도 고마워~! 마지막으로 성희, 너 때문에 감사의 글 수정해서 논문제본 다시 하는 일 없도록 우리 잘 지내자~^^;

2008년 여름 박 원 필 올림.

## TABLE OF CONTENTS

LIST OF FIGURES.....	ii
LIST OF TABLES.....	iii
ABSTRACT (ENGLISH).....	iv
I. INTRODUCTION.....	1
II. MATERIALS & METHODS.....	4
Stent FE model.....	4
Balloon-catheter FE model.....	7
Normal & stenosed artery FE model.....	9
Constitutive material models.....	11
Boundary and contact conditions.....	11
Simulation of the transient non-uniform balloon-stent expansion.....	13
Validation of the FE simulations.....	14
Comparative study.....	15
A. Foreshortening and dogboning.....	15
B. Aperture areas.....	16
III. RESULTS.....	17
Accuracy of the FE simulation.....	17
Foreshortening and dogboning of the seven commercial stents.....	20
A. At the free expansion.....	20
B. At the normal artery.....	23
C. At the 36% stenosed artery.....	26
D. At the 64% stenosed artery.....	29
Inner arterial wall stress of the seven commercial stents.....	32
Aperture area of the seven commercial stents.....	34
IV. DISCUSSIONS & CONCLUSIONS.....	35
REFERENCES.....	39
ABSTRACT (KOREAN).....	42
AUTHOR'S ACCOMPLISHMENTS.....	43

## LIST OF FIGURES

Figure 1. Final three-dimensional FE models of the seven commercial stents. ....	5
Figure 2. Final three-dimensional FE model of the balloon for the stent and its schematic diagram at a cutaway cross-sectional view used to illustrate the tri-folded membrane in the unit folder and the structural parameters of the balloon. ....	8
Figure 3. Final three-dimensional FE models of normal & stenosed arteries. ....	10
Figure 4. Boundary and contact condition used in finite element analysis. ....	12
Figure 5. Five POIs used for to validate the FE simulation for the transient non-uniform balloon-stent expansion process. The relationship between the internal pressure and the diameter of the balloon-stent during the transient non-uniform balloon-stent expansion process was identified using the FE predictions at the POIs. ....	14
Figure 6. Illustration of terms used for calculation of area per aperture. ....	16
Figure 7. Process of real transient non-uniform balloon-stent expansion. <sup>44</sup> ....	18
Figure 8. Pattern of the transient non-uniform balloon-stent expansion at four different instants during the expansion process. Only the expansion pattern for the Palmaz-Schatz PS153 stent is shown a) before expansion, b) and c) during expansion, and d) after expansion. ....	18
Figure 9. Pressure-diameter curve during the transient non-uniform balloon-stent expansion process obtained from the stents analyzed in the literature <sup>5, 24</sup> and the current study. ....	19
Figure 10. Forshortening (%) along with radial internal pressure (MPa) during the transient non-uniform balloon-stent expansion process obtained from the stents analyzed at the free expansion. ....	22
Figure 11. Dogboning (%) along with radial internal pressure (MPa) during the transient non-uniform balloon-stent expansion process obtained from the stents analyzed at the free expansion. ....	22
Figure 12. Forshortening (%) along with radial internal pressure (MPa) during the transient non-uniform balloon-stent expansion process obtained from the stents analyzed at the normal artery. ....	25
Figure 13. Dogboning (%) along with radial internal pressure (MPa) during the transient non-uniform balloon-stent expansion process obtained from the stents analyzed at the normal artery. ....	25

Figure 14. Forshortening (%) along with radial internal pressure (MPa) during the transient non-uniform balloon-stent expansion process obtained from the stents analyzed at the 36% stenosed artery. ....	28
Figure 15. Dogboning (%) along with radial internal pressure (MPa) during the transient non-uniform balloon-stent expansion process obtained from the stents analyzed at the 36% stenosed artery. ....	28
Figure 16. Forshortening (%) along with radial internal pressure (MPa) during the transient non-uniform balloon-stent expansion process obtained from the stents analyzed at the 64% stenosed artery. ....	31
Figure 17. Dogboning (%) along with radial internal pressure (MPa) during the transient non-uniform balloon-stent expansion process obtained from the stents analyzed at the 64% stenosed artery. ....	31
Figure 18. Inner wall stress (MPa) along with radial internal pressure (MPa) during the transient non-uniform balloon-stent expansion process obtained from the stents analyzed at the all artery. ....	33

## LIST OF TABLES

Table 1. Structural specifications of the seven commercial stents analyzed in the current study, determined based on the manufactures' specifications. ....	6
Table 2. Morphological construction and a number of nodes and elements of seven commercial stents. ....	6
Table 3. Summarized quantitative results of the foreshortening and dogboning behaviors of the seven commercial stents at the free expansion. ....	21
Table 4. Summarized quantitative results of the foreshortening and dogboning behaviors of the seven commercial stents at the normal artery. ....	24
Table 5. Summarized quantitative results of the foreshortening and dogboning behaviors of the seven commercial stents at the 36% stenosed artery. ....	27
Table 6. Summarized quantitative results of the foreshortening and dogboning behaviors of the seven commercial stents at the 64% stenosed artery. ....	30
Table 7. Summarized quantitative results of the aperture area of the seven commercial stents. ....	34

## ABSTRACT

### **The Study of Intravascular Stent Design Parameters to Reduce Restenosis Risk by Considering A Transient Non-uniform Balloon-Stent Expansion**

*Won-Pil Park*

Department of Biomedical Engineering  
The Graduate School, Yonsei University

*(Directed by Professor Han-Sung Kim, Ph. D)*

The foreshortening or dogboning of a stent that occurs due to transient non-uniform balloon-stent expansion can induce an intravascular injury, resulting in restenosis of the artery. However, previous studies rarely considered the effects of transient non-uniform balloon expansion on analysis of the mechanical properties and behaviors of stents during stent deployment, nor did they determine design parameters to minimize the restenosis risk driven by foreshortening or dogboning, nor did they determine design parameters to minimize the inner arterial wall stress value. The aim of the current study was, therefore, to suggest potential design parameters capable of reducing the possibility of restenosis risk driven by foreshortening or dogboning and decreasing of inner arterial wall stress value through a comparative study of seven commercial stents using finite element (FE) analyses of a realistic transient non-uniform balloon-stent expansion process. The results indicate that using stents composed of opened unit cells connected by bend-shaped link structures and controlling the geometrical and morphological features of the unit cell strut or the link structure at the distal ends of stent may prevent restenosis risk caused by foreshortening or dogboning. And also, the results indicate that using stents composed of opened unit cells connected by bend-shaped link structures with limited aperture area and controlling the geometrical and morphological features of the unit cell strut or the link structure of stent may decrease inner arterial wall stress value. This study provides a first look at the realistic transient non-uniform balloon-stent expansion by investigating the mechanical properties, behaviors, and design parameters capable of reducing the possibility of restenosis risk induced by the foreshortening or the dogboning.

---

**Keywords** : Intravascular stent, Foreshortening, Dogboning, Transient non-uniform balloon expansion, Finite element analysis



## I. INTRODUCTION

Intravascular diseases are serious healthcare problems in the present day. In the United States, coronary artery diseases are one of the principal causes of mortality, with a socioeconomic burden estimated to reach \$400 billion in 2006.<sup>1</sup> Atherosclerosis, also known as an coronary artery disease, is one of the most serious forms of coronary artery disease that affects the coronary artery.<sup>1,2</sup> It is characterized by a chronic inflammatory response in the arterial inner wall, in large part due to the deposition of lipoproteins (atheromatous plaques known as plasma proteins that carry cholesterol and triglycerides). This leads to a thickening of the inner arterial walls, resulting in the reduction of blood flow by narrowing or even blocking (restenosis) the arteries.

Currently, three of the most common treatments for coronary artery diseases that do not respond to pharmacologic therapy are coronary artery bypass grafting (CABG), percutaneous transluminal coronary balloon angioplasty (PTCA), and percutaneous transluminal coronary stenting with the aid of balloon angioplasty (PTCA with stent). Of these, at present, the intravascular intervention market for stents has increased rapidly because of their high initial success rate, minimal invasive nature, and improved long-term effectiveness compared to coronary artery bypass grafting or percutaneous transluminal coronary balloon angioplasty.<sup>3,4</sup> <sup>5</sup> Each year, over one million percutaneous interventions are performed worldwide, exceeding the annual number of coronary artery bypass grafts. The use of stents in interventional procedures has rapidly increased from 10% in 1994 to over 80% in current practice.<sup>5,6</sup> In a recent review of randomized trials comparing the stenting technique with balloon angioplasty, the stenting technique reduced the rates of revascularization by 35 to 75%, while angiographic indexes of the restenosis decreased by 20 to 55%.<sup>6,7</sup>

Stent generally features either an expandable wire or perforated tube that is inserted into an artery to prevent or counteract a disease-induced localized blood flow constriction. The first stent was introduced and implanted by Dotter<sup>8</sup> to treat arterial shrinkage. Clinical utilization of stents has been widely accepted in the 1990s to improve the limitations of balloon angioplasty, such as restenosis and abrupt closures of the arteries.<sup>9, 10</sup> However, potential limitations, such as restenosis,<sup>3, 4, 11</sup> migrations,<sup>12, 13</sup> collapses,<sup>14, 15</sup> or positioning difficulties<sup>16</sup> are still seen in clinical utilization of stents. Among these potential limitations, restenosis has become the main bottleneck to the development of stenting techniques.<sup>5, 17</sup>

There are several mechanisms that lead to restenosis. The principal etiology of restenosis is inflammatory response around the angioplasty site, which induces a tissue proliferation

(neointimal hyperplasia) around the angioplasty site.<sup>18, 19</sup> Moreover, these inflammatory responses were caused by fracture of the internal elastic lamina, dissection of the media, and often extending into the adventitia during stent expansion.<sup>20, 21, 22, 23</sup> At the view point of mechanical properties of stent, major factors of injury-inducing at inner artery wall are the foreshortening and the dogboning.<sup>5, 24</sup> And, mechanical properties and inner artery properties of stent are related to the design parameters of stent.<sup>5, 24, 25, 26</sup> Kastrati et al.<sup>18</sup> showed that the incidence of restenosis ranged from 20 to 50%, depending on the stent design, in a clinical study of 4,510 stent placements. Issues with respect to the design of intravascular stents generally include: 1) radial stiffness, 2) flexibility, 3) minimal foreshortening (contraction in length of the stent as dilating the stent), 4) minimal dogboning (larger expansion in diameter at the distal point compared with that at the central point of the stent as dilating the stent: flaring of stent ends), 5) minimal longitudinal recoil, 6) minimal radial recoil 7) minimal coverage area, and 8) fatigue durability.<sup>5, 27</sup> These issues are related directly or indirectly to restenosis.

It is widely accepted that finite element (FE) analysis is powerful tools for rapid investigation and improvement of design concepts prior to clinical trials. Rogers et al.<sup>28</sup> studied a two-dimensional balloon-artery interaction during stent placement. Dumoulin and Cochelin<sup>29</sup> evaluated and characterized the mechanical properties and behaviors of a balloon expandable stent. Etave et al.<sup>27</sup> compared the performance of two types of stents. Berry et al.<sup>30</sup> assessed the hemodynamics and wall mechanics of compliance matching stents in a stent-artery hybrid structure. Chua et al.<sup>2, 31, 32, 33</sup> investigated stent expansion, balloon-stent interaction, expansion characteristics of slotted tube stents in the presence of plaques and arteries, and the effect of varying the slotted tube stent geometry on its expansion behavior. Auricchio et al.<sup>34</sup> studied the biomechanical interaction between a balloon-expandable stent and a stenotic artery using three-dimensional FE analysis. Lally et al.<sup>35</sup> assessed the different levels of stress and different restenosis rates in the arterial inner wall with plaque induced by two different stent designs. Walke et al.<sup>36</sup> investigated the stent expansion process and mechanical properties of the intravascular stent in the blood vessel by the experimental and numerical research. Takashima et al.<sup>37</sup> studied the characterization of the stress distribution at the contact area between the stent and the artery using the mathematical and experimental modeling. Gay et al.<sup>38</sup> investigated the mechanical behaviors of angioplasty stents during and after implantation using a fluid–structure interaction computational technique. Migliavacca et al.<sup>10, 39, 40</sup> assessed the mechanical properties and behavior of balloon-expandable stents to determine how the FE method could be used to optimize stent designs. They also compared the performance of stainless steel stents with shape memory alloy stents

by analyzing the stress on the inner arterial wall induced by the expansion of balloon-expandable stents and self-expandable stents, and demonstrated how the mechanical properties and behaviors of new generation balloon-expandable stents could be studied accurately with computational analyses based on the FE method. Wang et al.<sup>5</sup> investigated the transient expansion behavior of six models of balloon-expandable stents and proposed a new modified stent based on their comparative study.

Previous studies have not, however, investigated transient non-uniform balloon expansion during stent deployment. They thought that it seemed justifiable to model balloon expansion by considering uniform radial internal pressure. Such assumption was based on the fact that stent is almost uniformly dilated and finally evenly expanded. That was only true away from the ends of the stent. Therefore, in order to fully understand the mechanical properties and behaviors of stent, it is necessary to consider a realistic modeling of transient non-uniform balloon-stent expansion with FE analysis. Furthermore, previous studies have not considered a comparative inner wall stress states due to respective difference of stent design parameters.

Particularly, considering the realistic transient non-uniform balloon-stent expansion is especially important because an undesirable foreshortening or dogboning driven during stent deployment can initiate intravascular restenosis injuries. Thus, for the study of the mechanical properties and behaviors of foreshortening or dogboning of stent, the realistic transient non-uniform balloon-stent expansion should be considered. Moreover, it is important to consider not only mechanical characteristics but also inner wall stress related to stent design parameters.

The aim of the current study is to suggest potential design parameters capable of reducing a risk of intravascular restenosis injuries, which can be induced by the mechanical characteristics of stent such as foreshortening or dogboning and the intravascular injury due to high inner arterial wall stress, through a comparative study of recently developed seven commercial stents using FE analyses of the realistic transient non-uniform balloon-stent expansion process.

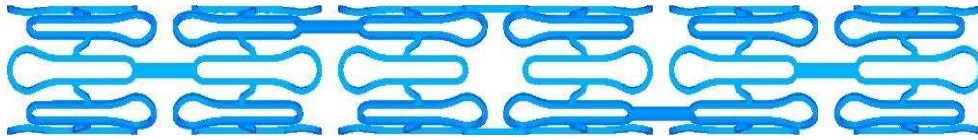
## II. MATERIALS & METHODS

### Stent FE model

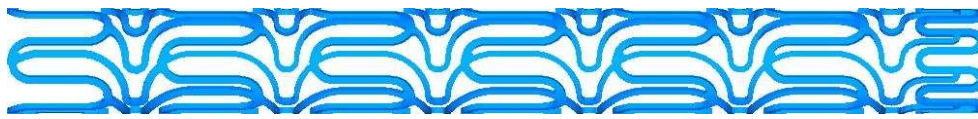
Three-dimensional FE models of seven commercial stents (Palmaz-Schatz PS153, Tenax<sup>TM</sup>, MAC Standard, MAC Q23, MAC Plus, Coroflex, RX Ultra Multi-link) were created using Hypermesh 7.0 (Altair Engineering, Inc., USA) (Fig. 1) based on the manufactures' specifications. The structural specifications of the stents are summarized in Table 1. The Palmaz-Schatz PS 153 stent (Johnson and Johnson Co., USA) was manufactured as a tubular structure composed of a closed rectangular unit cell without a link structure in the longitudinal direction of the stent (Fig. 1a). The Tenax<sup>TM</sup> stent (Biotronik, Germany) had a tubular structure composed of a closed unit cell with a corrugated ring pattern and an independent bar link structure in the longitudinal direction of the stent (Fig. 1b). The MAC Standard stent (amg GmbH, Germany) had a tubular structure composed of an opened unit cell with a sinusoidal curvature and an independent link structure of a bend-shaped connector arranged asymmetrically in the longitudinal direction of the stent (Fig. 1c). The MAC Q23 and Plus stents (amg GmbH, Germany) and the Coroflex stent (B. Braun Melsunen AG, Germany) had a tubular structure composed of an opened unit cell with a sinusoidal curvature and an independent link structure of a bend-shaped connector arranged symmetrically in the longitudinal direction of the stent (Fig. 1d-f). The RX Ultra Multi-link stent (Guidant, USA) was composed of a tubular structure connected by an opened unit cell with a corrugated wave pattern and an independent straight-line link structure arranged in the longitudinal direction of the stent (Fig. 1g). The final FE models of the stents consisted of 16,320 to 27,584 eight-node linear brick solid elements (C3D8R). The morphological construction and a number of nodes and elements of seven commercial stents were summarized in Table 2. Here, two layers of elements were considered for representation of the strut thickness of the stent. One layer of the strut of the stents was therefore consisted of 8,160 to 13,792 eight-node linear brick solid elements. To avoid inaccuracy of FE results due to improper mesh on the curved portion of the FE model, a great number of elements were incorporated into the curved portion compared with elements used for the straight portion of the strut of the stent. Here, the ratio of the elements incorporated into the curved to the straight portions was average 2 to 1.



a) Palmaz-Schatz PS 153 stent (Johnson and Johnson Co., USA)



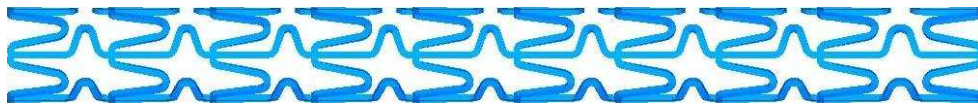
b) Tenax™ stent (Biotronik, Germany)



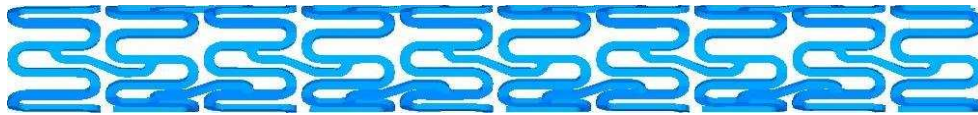
c) MAC Standard stent (amg GmbH, Germany)



d) MAC Q23 stents (amg GmbH, Germany)



e) MAC Plus stents (amg GmbH, Germany)



f) Coroflex stent (B. Braun Melsunen AG, Germany)



g) RX Ultra Multi-link stent (Guidant, USA)

Figure 1. Final three-dimensional FE models of seven commercial stents.

Table 1. Structural specifications of the seven commercial stents analyzed in the current study, determined based on the manufactures' specifications.

Stent \ Item	General Structural Parameters for the Stent				Unit Cell Structural Parameters	Structural Parameters in the Link Structure	
	Outer Diameter (mm)	Inner Diameter (mm)	Strut Thickness (mm)	Length (mm)	Strut Width (mm)	Strut Width (mm)	Strut Length (mm)
Palmaz-Schatz PS153	1.484	1.389	0.095	16.0	0.106	0.106	3.720
Tenax	1.780	1.695	0.085	15.1	0.083	0.199	0.834
MAC Standard	1.800	1.715	0.085	16.8	0.125	0.125	3.581
MAC Q23	1.800	1.715	0.085	16.8	0.126	0.100	2.764
MAC Plus	1.764	1.669	0.095	15.0	0.125	0.125	3.487
Coroflex	1.725	1.630	0.095	15.9	0.136	0.135	1.647
RX Ultra Multi-link	1.764	1.669	0.095	15.0	0.097	0.096	1.382

Table 2. Morphological construction and a number of nodes and elements of seven commercial stents.

Stent \ Item	Type of Unit Cell	Type of Link Structure	Number of Nodes	Number of Elements
Palmaz-Schatz PS153	Closed	No Connector	31558	13956
Tenax		Bar	34965	15720
MAC Standard	Opened	Bend Shaped	30795	14180
MAC Q23			36819	16760
MAC Plus			38052	18048
Coroflex			58563	26118
RX Ultra Multi-link		Straight Line	59742	27584

### Balloon-catheter FE model

The three-dimensional FE model of the stent balloon was also built using Hypermesh 7.0 based on the actual contours of the balloon (Fig. 2). During the initial phase of expansion, the balloon was represented by folding the membrane into a unit cell (hereafter called the “unit folder”) as shown in Fig. 2a. Then, five unit folders were considered in a cutaway cross-sectional view. For each unit folder, the membrane was tri-folded, resulting in the formation of three layers, based on the fact that an actual balloon is usually tri-folded before being crimped onto the stent<sup>5</sup> and on the necessary and sufficient condition that the membrane must be unfolded completely at the final phase of the expansion. The outer radius of the balloon ( $r_1$ , from the first membrane layer to the center of the balloon), middle radius of the balloon ( $r_2$ , from the second membrane layer to the center of the balloon), and inner radius of the balloon ( $r_3$ , from the third membrane layer to the center of the balloon) were about 0.59, 0.56, and 0.53mm, respectively, and the lengths of the first ( $d_1$ ), second ( $d_2$ ), and third ( $d_3$ ) membranes were 0.74, 0.71, and 0.68mm, respectively. These yielded a target balloon diameter ( $d_p$ ) of about 3.60 mm at the final phase of the expansion, which is larger than a typical original coronary artery diameter. In generally, typical original coronary artery diameter is about 3.00mm.<sup>5,10</sup> However, larger scale balloon diameter (3.60mm) was applied for apparent effect during stent deployment in this study. Other structural parameters and their values considered in the current study are shown in Fig. 2. The final FE models of the balloon consisted of 10,700 four-node shell elements (S4R) and 10,700 four-node hydrostatic fluid elements (F3D4) (Fig. 2). A thickness of 0.033mm measured from the actual membrane of the balloon was assigned to the shell elements. The hydrostatic fluid elements were used to simulate the balloon expansion by changing the amount of fluid in a fluid-filled cavity. This process will be explained in detail below.

The shaft in the catheter that allows fluid to be injected into the balloon was developed as a rigid body to establish a datum point for the balloon expansion (Fig. 2). The diameter of the shaft was matched to the caliber of the balloon, and the length of the shaft was slightly larger than that of the balloon (Fig. 2).

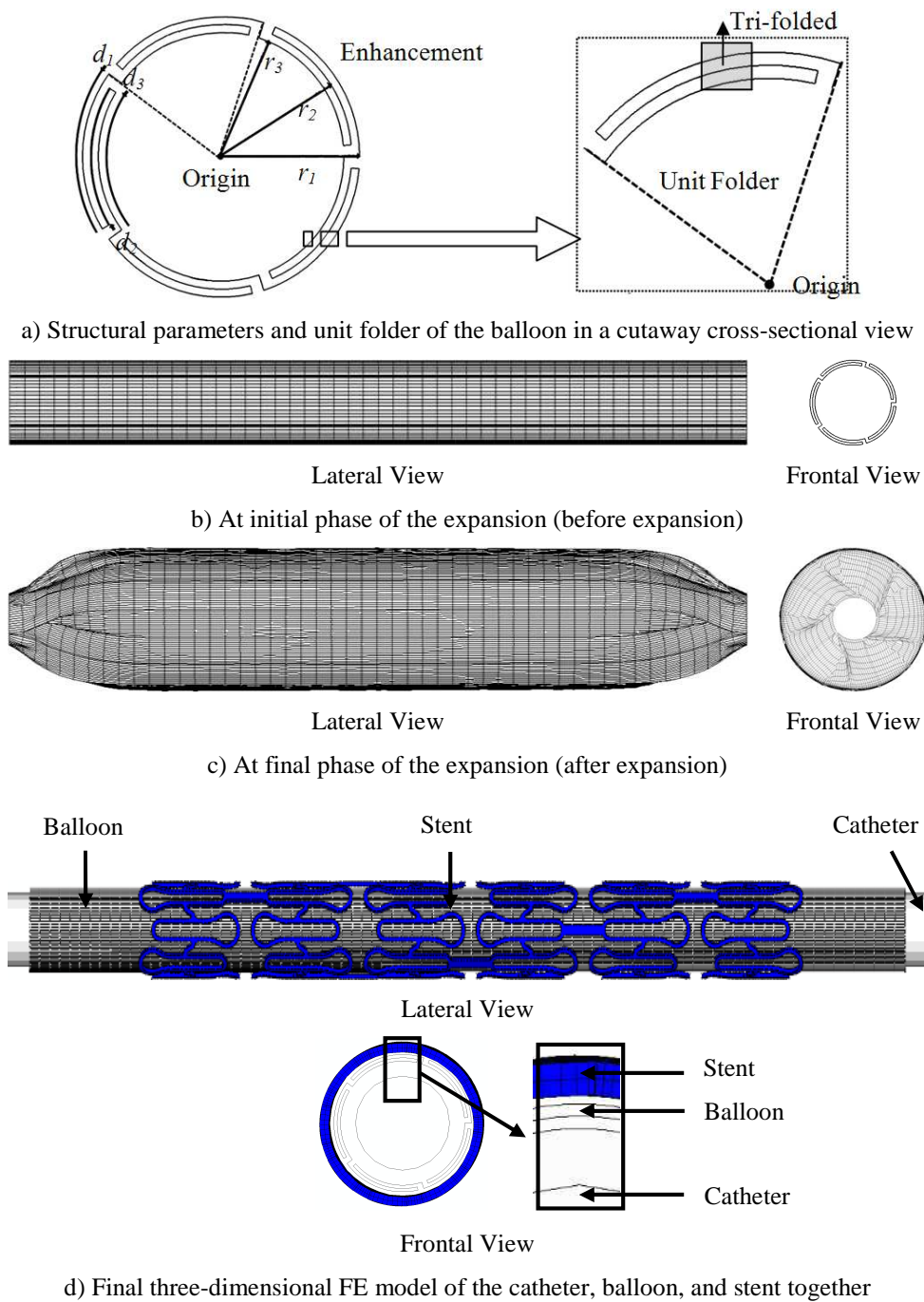


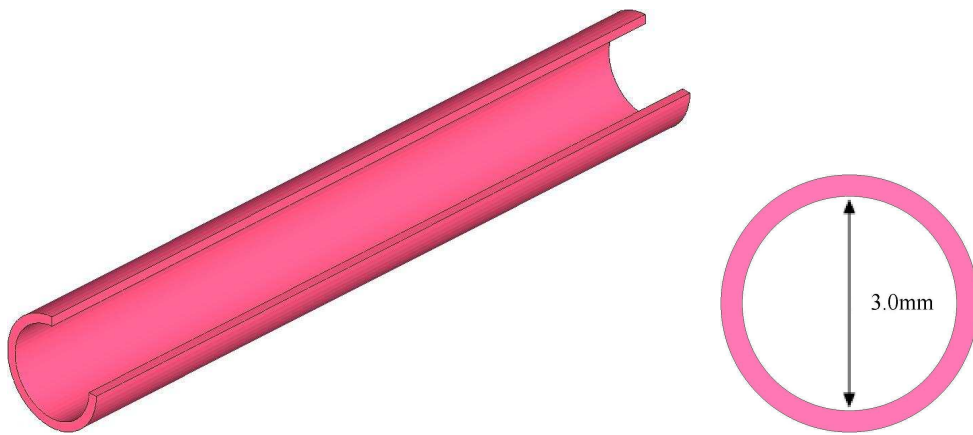
Figure 2. Final three-dimensional FE model of the balloon for the stent and its schematic diagram at a cutaway cross-sectional view used to illustrate the tri-folded membrane in the unit folder and the structural parameters of the balloon.



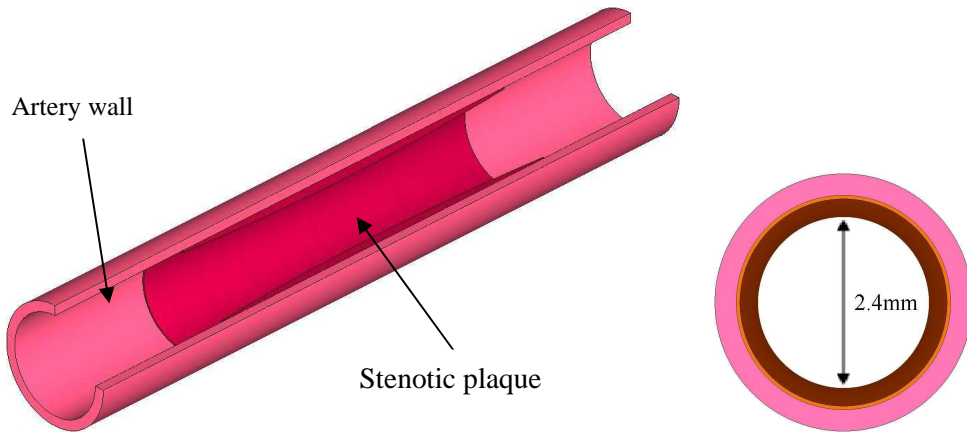
### **Normal & stenosed artery FE model**

The three dimensional FE model of normal artery and stenosed artery were also built using Hypermesh 7.0 based on the literature (Fig. 3).<sup>35</sup> The normal artery was modeled as an idealized vessel and represented by a cylinder with outer diameter of 3.6mm (inner diameter : 3mm, thickness : 0.3mm) (Fig. 3a). Length of normal artery model was different with each stent. To avoid the trouble related to expansion (e.g. secession of stent-balloon FE model and artery FE model), it has about 5mm longer than stent's length to both ends. The stenosed arteries were modeled as normal artery with a localized crescent shaped axisymmetric stenosis with minimum lumen diameter of 1.8mm and 2.4mm (Fig. 3b-c). The plaque corresponds to a maximum stenosis of about 36% and 64% of the proximal and distal lumen cross-sectional area. For a precise measuring of foreshortening, length of plaque was same as each stent's length. The final FE models of the normal artery consisted of 31,563 to 35,154 eight-node linear brick solid elements (C3D8R). Here, three layers of elements were considered for representation of the thickness of the normal artery. One layer of the artery was therefore consisted of 10,521 to 11,718 eight-node linear brick solid elements. And also, stenosed artery consisted of 124,866 to 136,556 (36% stenosed model) and 156,366 to 167,516 (64% stenosed model) eight-node linear brick solid elements. As similar as a normal artery, two layers of elements were considered for representation of the thickness of the stenosed artery. One layer of the plaque was therefore consisted of 62,433 to 68,278 (36% stenosed model) and 78,183 to 83,758 (64% stenosed model) eight-node linear brick solid elements.

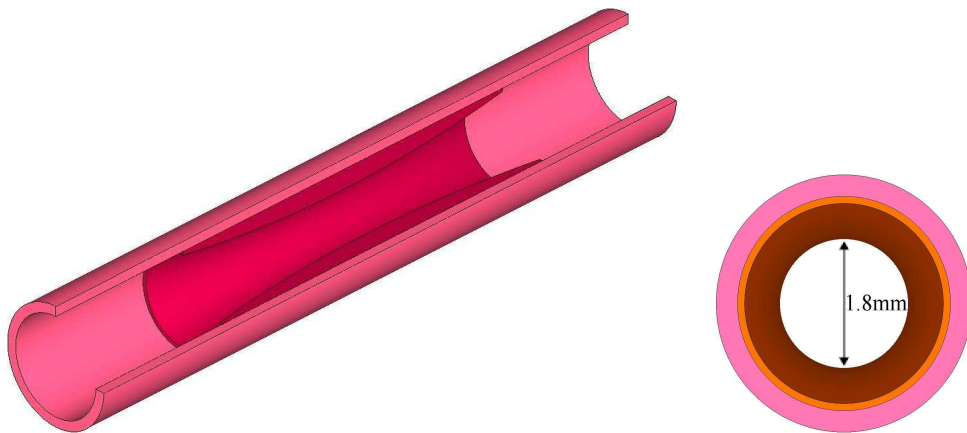
To prevent an inaccuracy of FE results due to irregular mesh size of artery FE model, a size of constituent elements of every artery FE models were similar. Here, the volume of the elements were about  $2.5\mu\text{m}^3$ .



a) Normal artery (Inner diameter : 3.0mm)



b) 36% stenosed artery (Minimum inner diameters : 2.4mm)



c) 64% stenosed artery (Minimum inner diameters : 1.8mm)

Figure 3. Final three-dimensional FE models of normal & stenosed arteries. Thickness of artery wall is 0.3mm.

### Constitutive material models

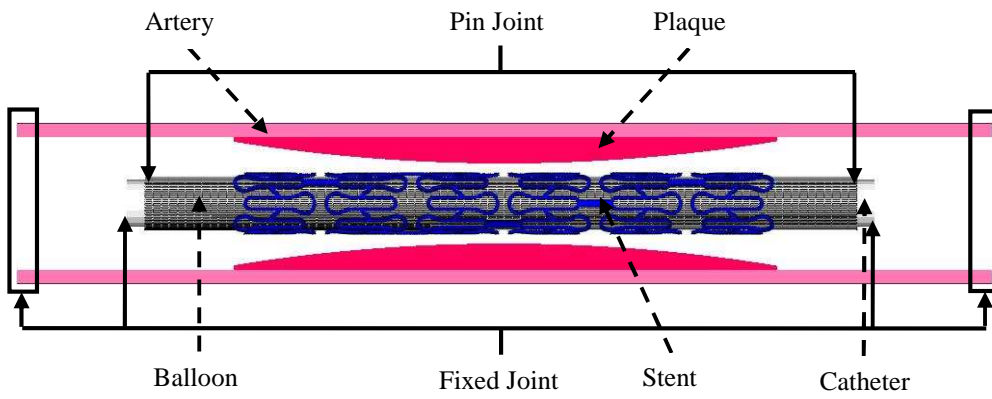
The stents were assumed to be made of stainless steel 316L, which had an elasto-plastic constitutive behavior obtained from an engineering stress-strain curve reported by Albertini and Montagnani.<sup>41</sup> The general mechanical properties of this material were 196GPa for the elastic modulus ( $E$ ), 308MPa for the yield stress ( $Y_s$ ), and 0.33 for the Poisson ratio ( $\nu$ ).<sup>41</sup>

The balloon was assumed to be made of high-density polypropylene that had an isotropic linear elasticity. The mechanical properties of the material were then determined from the literature ( $E$ : 1GPa,  $Y_s$ : 90MPa, and  $\nu$ : 0.33).<sup>42</sup>

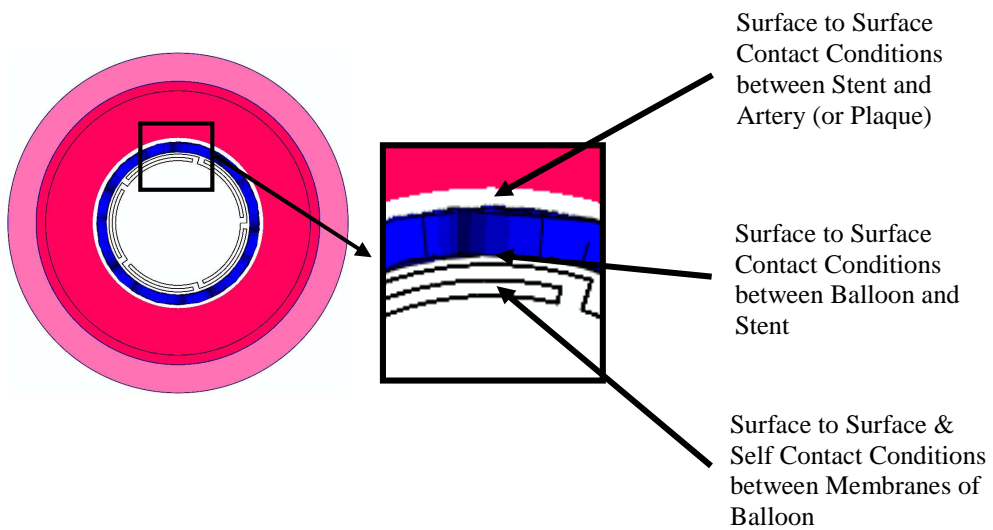
The artery and the plaque were modeled using a 5-parameter third-order Mooney–Rivlin hyperelastic constitutive equation. Mooney–Rivlin hyperelastic model has been found to adequately describe the non-linear stress-strain relationship of elastic arterial tissue.<sup>43</sup> The material properties of the artery ( $A_{10}$ : 18.90KPa,  $A_{01}$ : 12.7KPa,  $A_{20}$ : 85.72KPa,  $A_{11}$ : 590.43KPa, *Other Values*: 0KPa) and plaque ( $A_{10}$ : -495.96KPa,  $A_{01}$ : 506.61KPa,  $A_{20}$ : 1193.53KPa,  $A_{11}$ : 3637.8KPa,  $A_{30}$  : 4737.25KPa, *Other Values*: 0KPa) were then determined from the literature.<sup>35</sup>

### Boundary and contact conditions

Three boundary conditions were assigned to the ends of the balloon, to the shaft of the catheter and to the ends of the artery, and four contact conditions were used between the folded membranes of the balloon, between the stent and the balloon, between the stent and the artery (or plaque) and between the balloon and the artery (or plaque) (Fig. 4). A pin joint boundary condition was used for the balloon based on the fact that the balloon generally expands to an ellipsoid form, as shown in Fig. 4. A fixed joint boundary condition was assigned to the rigid-body shaft of the catheter to avoid movement of the catheter in all directions during the balloon expansion. A fixed joint boundary condition was also assigned to the ends of the artery to avoid movement of the artery in all directions during the balloon expansion. Surface-to-surface contact conditions were used between the stent and the balloon, between the stent and the artery (or plaque) and between the balloon and the artery (or plaque), while surface-to-surface and self-contact conditions were used for the folded membranes during the expansion of the balloon.



a) Boundary conditions



b) Contact conditions

Figure 4. Boundary and contact conditions used in finite element analysis.

### **Simulation of the transient non-uniform balloon-stent expansion**

The transient non-uniform balloon simulation was performed in three steps. First, the simulation mimicked the free expansion of the stent until the initial radius ( $r_l = 0.59\text{mm}$ ) of the balloon reached the value of the initial inner radius of the stents ( $r_s = 0.69\text{mm}$  for the Palmaz-Schatz PS153 stent,  $0.85\text{mm}$  for the Tenax<sup>TM</sup> stent,  $0.86\text{mm}$  for the MAC Standard and Q23 stents,  $0.83\text{mm}$  for the MAC Plus stent,  $0.82\text{mm}$  for the Coroflex stent, and  $0.83\text{mm}$  for the RX Ultra Multi-link stent). Second, the simulation was used to examine dogboning to a diameter of  $3.6\text{mm}$ , corresponding to a slightly larger than the typical inner diameter of an artery.<sup>5, 10</sup> Finally, the simulation was used to investigate foreshortening after the balloon was removed. The stents were then unloaded, decreasing the internal pressure to zero. The definition of the mechanical properties and behavior will be explained in detail below.

The balloon-stent expansion was performed by controlling the features of the hydrostatic fluid elements. A pneumatic flow at  $15\text{atm}$  and surgical room temperature was used for the stent, with an amplitude option that allowed arbitrary time variations of the amount of fluid mass (fluid mass flow rate) to be supplied throughout the simulation. A fluid flux option was used to specify changes in the fluid mass of the fluid-filled cavity modeled with the hydrostatic fluid elements. Thus the balloon-stent expansion was controlled by a change in the amount of fluid mass (volume controlled process).

The ABAQUS 6.7 package (Dassault Systèmes, Inc., Providence, RI, USA) was used to solve the FE models. Both the explicit and implicit ABAQUS commercial packages on IBM p690 systems at KISTI Super Computing center (located at Yuseong-gu, Daejeon-si, Korea) were used for all steps.

## Validation of the FE simulations

Sensitivity (convergence) tests of the stent FE models were performed to identify the influence of the number of elements on the FE results. The number of elements for each stent FE model was 0.5 times decreased (coarsest mesh model) or 1.5 times increased (finest mesh model) gradually relative to the original mesh model (used in the current study), and the resulting foreshortening and dogboning values were examined and compared. Additional temporal sensitivity tests were also conducted by specifying explicit time integration for all stent FE models in the original mesh model. For this temporal sensitivity tests, time period of the step was altered from 130 to 170 at an interval of 10, and a degree of convergence of FE simulation for each time period and difference between the FE results obtained from the defined time periods were examined and compared with each other.

Validation of our FE simulations of stent-balloon expansions was performed by comparing our predicted expansion process, as well as the diameter and internal pressure at five points of interest (POIs) (Fig. 5) with experiment results analyzed from the literature.<sup>5, 24,</sup>

29

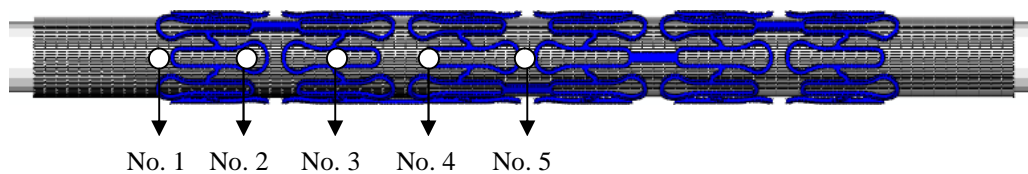


Figure 5. Five POIs used for to validate the FE simulation for the transient non-uniform balloon-stent expansion process. The relationship between the internal pressure and the diameter of the balloon-stent during the transient non-uniform balloon-stent expansion process was identified using the FE predictions at the POIs.

## Comparative study

### A. Foreshortening and dogboning

The evaluation of the stents focused on analyzing the mechanical properties and behaviors of foreshortening and dogboning, which could be influenced by the characteristics of the balloon-stent expansion, to identify potential design parameters that reduce restenosis induced by undesirable mechanical stress on the inner arterial wall.<sup>1, 5, 24, 29</sup> In general, the stent must be deployable to various locations in arteries in a simple and safe manner, and be capable of expanding the wall of the artery.<sup>1, 2, 5, 24, 27, 29, 31</sup> The stent must have a sufficiently high plastic ductility (indexed by flexibility or radial stiffness) and low elastic recoil (indexed by longitudinal or radial recoil).<sup>1, 10, 27, 29</sup> These mechanical requirements are of crucial importance and must be achieved by the specific design and material used for the stent to give a high tensile strength, yield strength, and ductile yield. However, the current study was focused on the mechanical properties and behaviors of foreshortening and dogboning.

The following equations<sup>5, 24</sup> were used to define foreshortening and dogboning:

$$\text{Foreshortening} = \frac{L - L^{load}}{L} \times 100\% \quad (1)$$

$$\text{Dogboning} = \frac{R_{POI}^{load} - R_{central}^{load}}{R_{distal}^{load}} \times 100\% \quad (2)$$

where  $L^{load}$ ,  $R_{central}^{load}$ , and  $R_{POI}^{load}$  are the longitudinal length, the central radius, and the radius at the POI of the stent, respectively, after the loading due to the stent-balloon expansion, and  $L$  is the initial length of the stent.

## B. Aperture areas

The evaluation of the stents focused on analyzing the inner arterial wall stress, which could be influenced by the geometrical and morphological characteristics, to identify potential design parameters that reduce restenosis induced by undesirable mechanical stress on the inner arterial wall.<sup>1, 10, 27, 29</sup> The following equation was used to define aperture areas:

$$\text{Area per aperture zone} = \frac{(\pi D_{\text{exp}} \times L_{\text{exp}}) - A_{\text{stent}}}{\text{Number of Aperture}} \quad (3)$$

where  $D_{\text{exp}}$ ,  $L_{\text{exp}}$ , and  $A_{\text{stent}}$  are the diameter of expanded stent, the length of expanded stent, contact area of expanded stent, respectively, after the loading due to the stent-balloon expansion (Fig. 6).

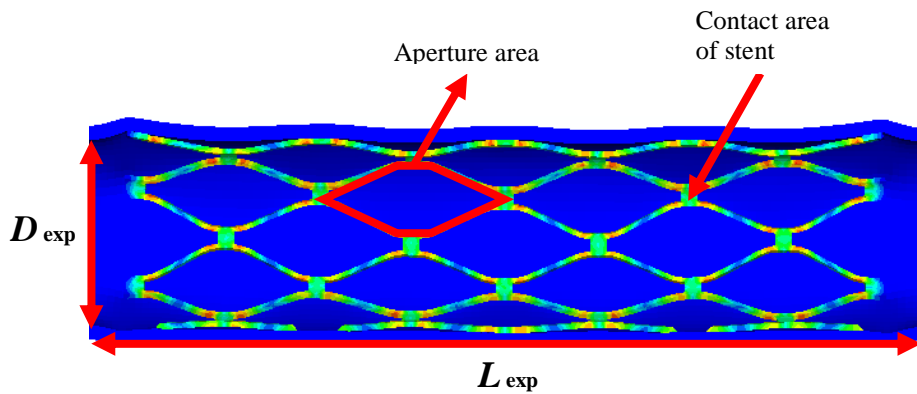


Figure 6. Illustration of terms used for calculating area per aperture.



### III. RESULTS

#### Accuracy of the FE simulation

The sensitivity test identifying the influence of the number of elements on the FE simulation results showed that the percent differences in the results between the original mesh and the other meshes were generally within approximately 0.4% for the coarsest mesh and approximately 0.2% for the finest mesh. This fact indicates that it is possible to conclude that a number of elements are not sensitive to the grid refinement of the mesh. The additional temporal sensitivity test performed by specifying explicit time integration showed that the FE simulation was convergent over 150 time period and the differences between the FE simulation results obtained over 150 time period were within almost 0%. These facts indicate that it is possible to conclude that the FE results are not sensitive to the time period over 150. Based on these facts, the original mesh and the 160 time period were used for all FE simulations performed in the current study. The process of real transient non-uniform balloon-stent expansion is shown in Fig. 7.<sup>44</sup> The pattern of the transient non-uniform balloon-stent expansion of our FE model at four different instants during the expansion process is shown in Fig. 8. Only the expansion pattern for Palmaz-Schatz PS153 stent is shown because all stents had similar expansion patterns. The radial displacement (volume change) in the distal region of the stent was larger than the central displacement at the second and third instants shown in the Fig. 8. b and c. However, the radial displacement in the distal region of the stent was equal to the central displacement at the fourth instant shown in the Fig. 8. d, corresponding to the final phase of the expansion. These results compared favorably with those reported in the literature.<sup>5, 24, 29</sup> The pressure-diameter curves for the transient non-uniform balloon-stent expansion process are shown in Fig. 9 for the balloon-stents analyzed in the current study. Results from the literature are also shown.<sup>5, 24</sup> In the period from the time that fluid was supplied to the balloon to the time that the balloon was fitted closely to the stent (Phase 1 in Fig. 9), our FE results indicated that the balloon diameter of all the stents was rarely changed. In the next stage (Phase 2 in Fig. 9) our FE results for all balloon-stents indicated a large increase in diameter with little increase in pressure, which corresponds to a burst-open or a chain-reaction deformation of the stent. This might indicate that the energy stored in the stent structure during the expansion of the stent was transformed into local plastic deformation so that the entire structure entered a state of plastic instability. Continuously, once all the weak parts of the stent had deformed plastically, further expansion required a high increase in pressure because of the limitation of the balloon expansion and the strain hardening of the stent material (Phase 3 in Fig. 9). The pressure-diameter curves predicted from our FE simulations for all balloon-stents compared favorably with those reported in the literature, as shown in Fig. 9.<sup>5, 24</sup>

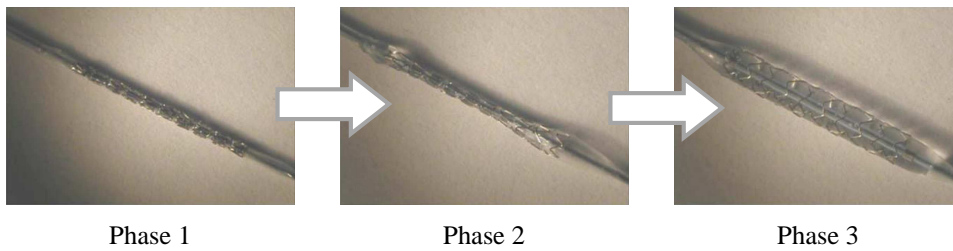


Figure 7. Process of real transient non-uniform balloon-stent expansion.<sup>44</sup>

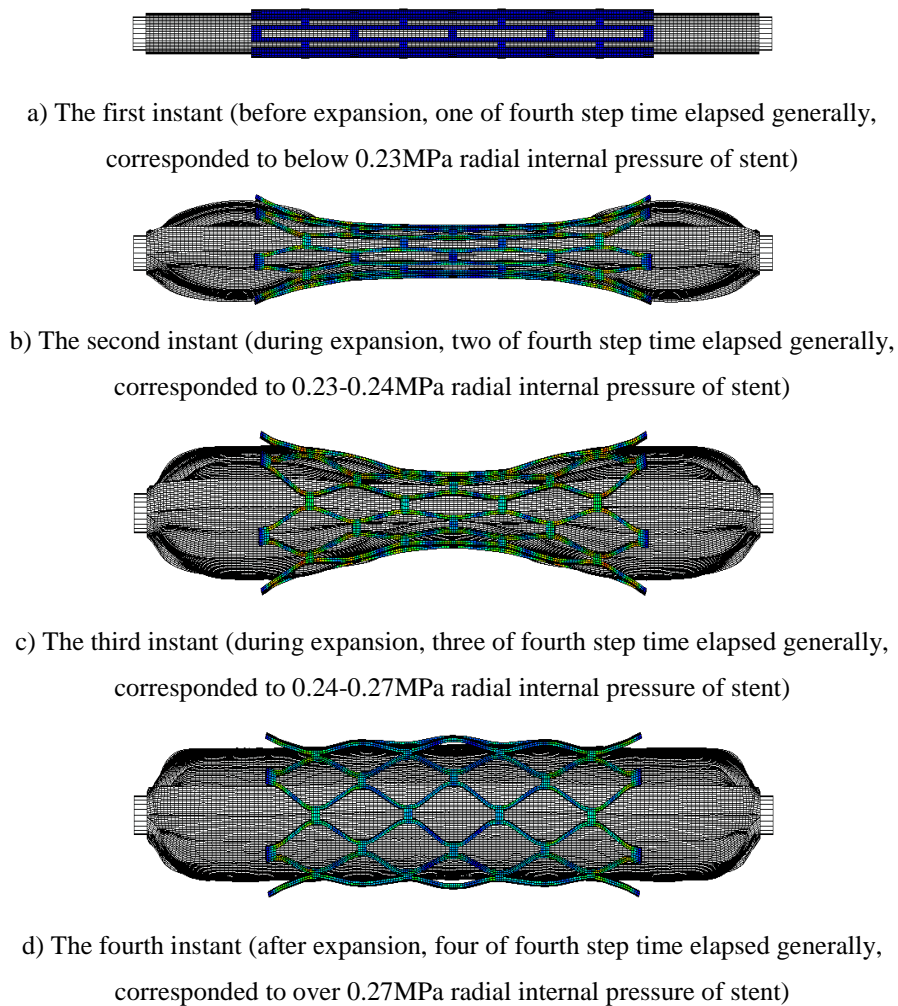


Figure 8. Pattern of the transient non-uniform balloon-stent expansion at four different instants during the expansion process. Only the expansion pattern for the Palmaz-Schatz PS153 stent is shown a) before expansion, b) and c) during expansion, and d) after expansion.

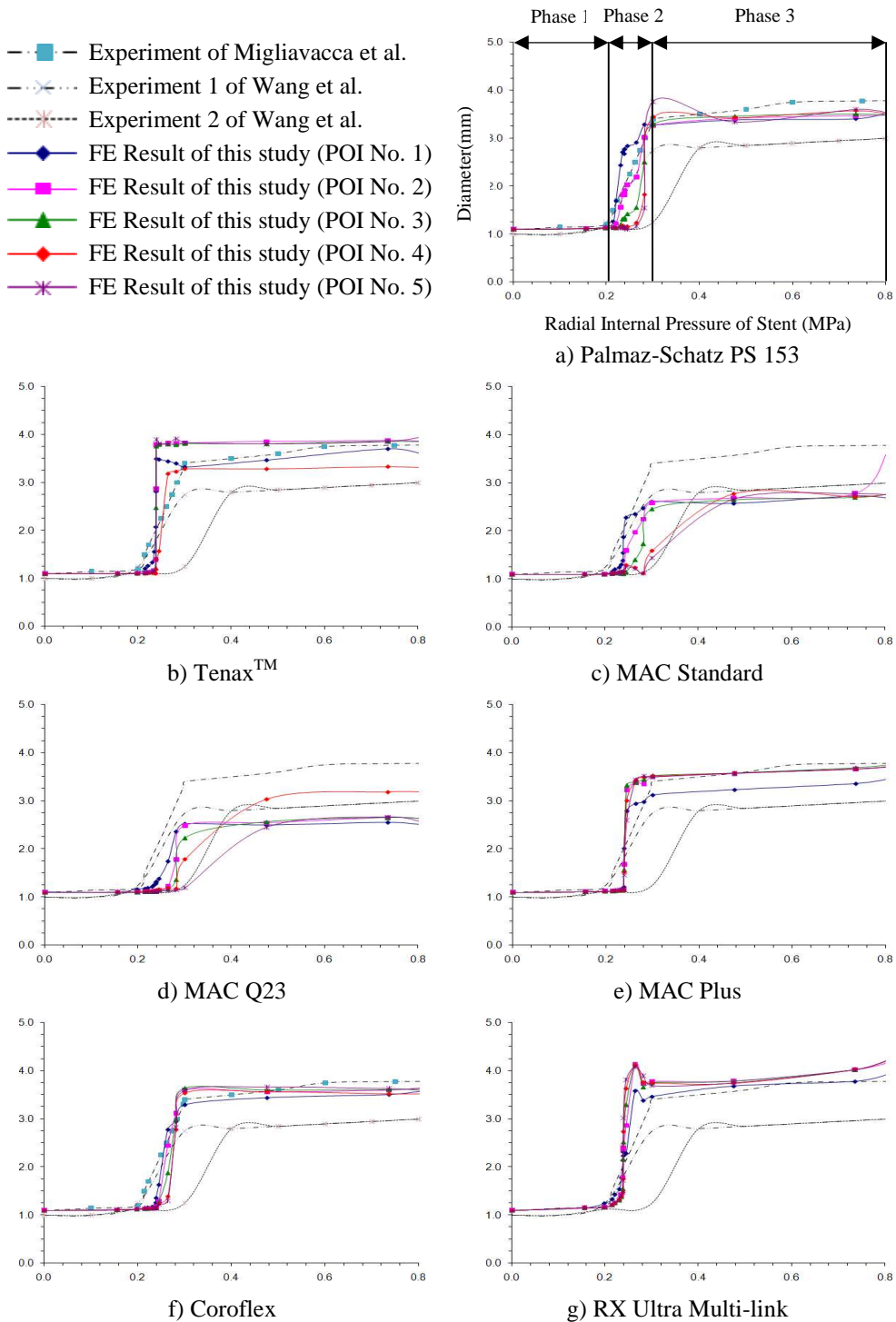


Figure 9. Pressure-diameter curve during the transient non-uniform balloon-stent expansion process obtained from the stents analyzed in the literature<sup>5, 24</sup> and the current study.

## **Foreshortening and dogboning of the seven commercial stents**

### **A. At the free expansion**

The foreshortening and dogboning results for the seven commercial stents at the free expansion are summarized in Table 3, and Fig. 10 and 11.

The foreshortenings, which depended on the geometrical and morphological characteristics of the stent, were ranged from 0.0% for the MAC Plus stent to 12.9% for the Tenax<sup>TM</sup> stent (Table 3 and Fig. 10). For all stents except to MAC Plus, the foreshortening was occurred abruptly at the radial internal pressure between 0.23MPa and 0.27MPa (corresponded to regime of the second and third instant appeared during the expansion of the stent shown in Fig. 8), and was remained in an almost constant value after the radial internal pressure of 0.27MPa (corresponded to regime of the fourth instant appeared during the expansion of the stent shown in Fig. 7) (Fig. 10). Generally, the stents with the closed unit cells connected to themselves or by a bar link structure (Palmaz-Schatz PS153, Tenax<sup>TM</sup>) had higher foreshortening values, whereas the stents with the opened unit cells connected by bend-shaped connector link structures (MAC Standard, MAC Plus, and Coroflex except to MAC Q23) or by an independent straight-line link structure (RX Ultra Multi-link) had lower foreshortening values (Table 3 and Fig. 10).

The dogboning values were positive for all balloon-stents, which indicates over-expansion of the distal points (i.e., POI No.1 – POI No.4) of the stent, i.e., when the balloon-stent expanded, the distal points and the central point (POI No.5) of the stent were spread out sequentially (Table 3 and Fig. 8 and 11). The maximum dogboning value for each stent was ranged from 19.4% for the MAC Plus stent to 64.3% for the Palmaz-Schatz PS153 stent (Table 3 and Fig. 11). For the POIs (POI No.1 – POI No.4) of all stents, the dogboning was occurred suddenly at the radial internal pressure between 0.23MPa and 0.27MPa (corresponded to regime of the second and third instant appeared during the expansion of the stent shown in Fig. 8), and was reduced and remained in an almost constant value after the radial internal pressure of 0.27MPa (corresponded to regime of the fourth instant appeared during the expansion of the stent shown in Fig. 8), similar to the foreshortening results (Fig. 11). Generally, for the POI No. 1, the stents with the closed unit cells connected to themselves (Palmaz-Schatz PS153) had higher dogboning value over 60%, whereas the stents with the closed unit cells connected by a bar link structure (Tenax<sup>TM</sup>) or with the opened unit cells connected by bend-shaped connector link structures (MAC Standard, MAC Q23, MAC Plus, and Coroflex) or by an independent straight-line link structure (RX Ultra Multi-link) had lower dogboning values below 60% (Table 3 and Fig. 11). Here, a tendency for the results of

the dogboning values for other POIs was similar to that for POI No. 1 (Table 3 and Fig. 11). Additionally, the results of the dogboning values showed that the stents with the closed unit cells connected to themselves (Palmaz-Schatz PS153) or with the opened unit cells connected by an independent straight-line link structure (RX Ultra Multi-link) had large differences among the dogboning values on the POIs (9.8-48.6% for Palmaz-Schatz PS153, 4.5-42.7% for RX Ultra Multi-link), whereas the stents the closed unit cells connected by a bar link structure (Tenax<sup>TM</sup>) or with the opened unit cells connected by bend-shaped connector link structures (MAC Standard, MAC Q23, and MAC Plus except to Coroflex) had relatively small differences among the dogboning values on the POIs (4.3-22.6% for Tenax<sup>TM</sup>, 1.2-26.5% for MAC Standard, 7.0-27.4% for MAC Q23, 2.2-11.6% for MAC Plus, 10.2-39.2% for Coroflex) (Table 3). Here, from the magnitude of the difference, a degree of injury risk on the inner arterial wall induced by the dogboning can be expected. That is, if the difference is small, the stent is expanded evenly at the distal points of the stent, resulting in a reduction of restenosis risk.

Table 3. Summarized quantitative results of the foreshortening and dogboning behaviors of the seven commercial stents at the free expansion.

Stent	Maximum Foreshortening (%)	Maximum Dogboning (%)			
		POI No. 1	POI No. 2	POI No. 3	POI No. 4
Palmaz-Schatz PS153	6.8	64.3	51.1	41.3	15.7
Tenax <sup>TM</sup>	12.9	46.4	42.1	33.3	23.7
MAC Standard	1.3	59.0	47.9	46.7	32.5
MAC Q23	7.2	54.3	46.8	33.9	26.9
MAC Plus	0.0	19.4	17.1	14.7	7.8
Coroflex	4.5	48.0	37.8	21.3	8.8
RX Ultra Multi-link	3.4	54.1	49.6	22.3	11.4

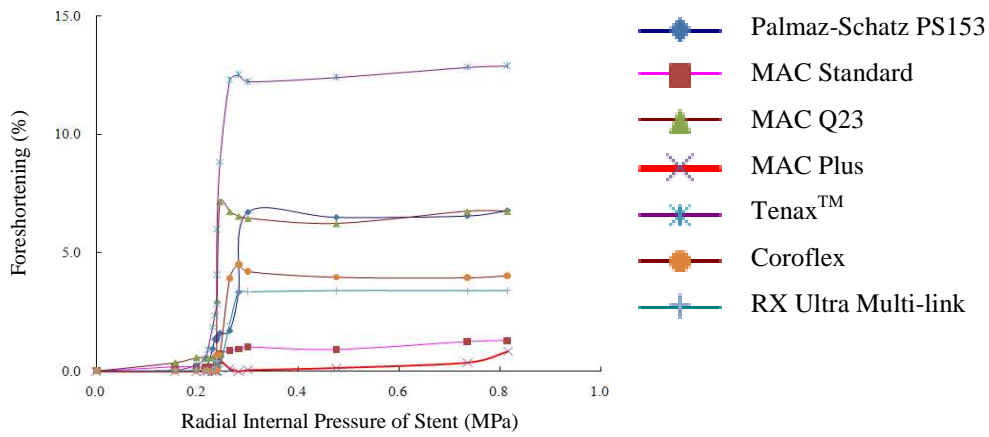


Figure 10. Forshortening (%) along with radial internal pressure (MPa) during the transient non-uniform balloon-stent expansion process obtained from the stents analyzed at the free expansion.

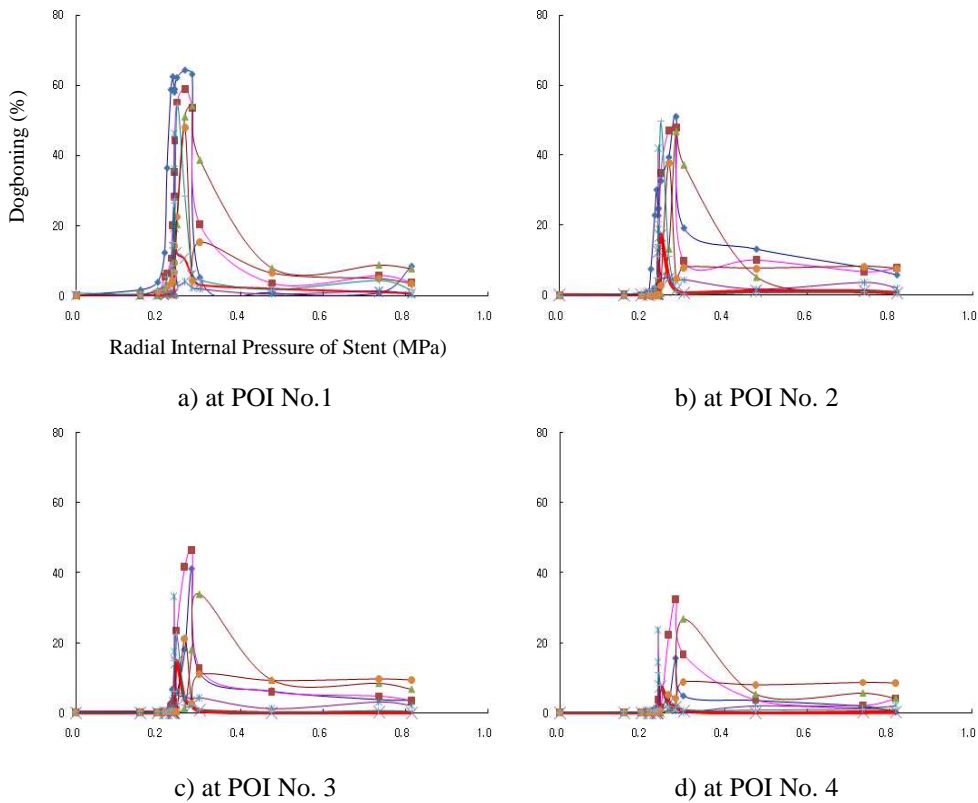


Figure 11. Dogboning (%) along with radial internal pressure (MPa) during the transient non-uniform balloon-stent expansion process obtained from the stents analyzed at the free expansion.

## **B. At the normal artery**

The foreshortening and dogboning results for the seven commercial stents at the normal artery are summarized in Table 4, and Fig. 12 and 13.

The foreshortenings, which depended on the geometrical and morphological characteristics of the stent, were ranged from 1.0% for the MAC Plus stent to 6.5% for the Palmaz-Schatz PS153 stent (Table 4 and Fig. 12). Contrary to results of free expansion, the foreshortening was occurred abruptly at the radial internal pressure between 0.23MPa and 0.27MPa (corresponded to regime of the second and third instant appeared during the expansion of the stent shown in Fig. 8), and was remained in an almost constant value after the radial internal pressure of 0.27MPa (corresponded to regime of the fourth instant appeared during the expansion of the stent shown in Fig. 8) for all stents (Fig. 12). Generally, the stents with the closed unit cells connected to themselves or by a bar link structure (Palmaz-Schatz PS153, Tenax<sup>TM</sup>) had higher foreshortening values, whereas the stents with the opened unit cells connected by bend-shaped connector link structures (MAC Standard, MAC Plus, and Coroflex except to MAC Q23) or by an independent straight-line link structure (RX Ultra Multi-link) had lower foreshortening values (Table 4 and Fig. 12).

The dogboning values were positive for all balloon-stents, which indicates over-expansion of the distal points (i.e., POI No.1 – POI No.4) of the stent, i.e., when the balloon-stent expanded, the distal points and the central point (POI No.5) of the stent were spread out sequentially (Table 4 and Fig. 8 and 13). The maximum dogboning value for each stent was ranged from 15.4% for the MAC Q23 stent to 56.9% for the Tenax<sup>TM</sup> stent (Table 4 and Fig. 13). For the POIs (POI No.1 – POI No.4) of all stents, the dogboning was occurred suddenly at the radial internal pressure between 0.23MPa and 0.27MPa (corresponded to regime of the second and third instant appeared during the expansion of the stent shown in Fig. 8), and was reduced and remained in an almost constant value after the radial internal pressure of 0.27MPa (corresponded to regime of the fourth instant appeared during the expansion of the stent shown in Fig. 8), similar to the foreshortening results (Fig. 13). Generally, for the POI No. 1, the stents with the closed unit cells (Palmaz-Schatz PS153, Tenax<sup>TM</sup>) had higher dogboning value over 50%, whereas the stents with the opened unit cells connected by bend-shaped connector link structures (MAC Standard, MAC Q23 and MAC Plus except to Coroflex) or by an independent straight-line link structure (RX Ultra Multi-link) had lower dogboning values below 50% (Table 4 and Fig. 13). Here, a tendency for the results of the dogboning values for other POIs was similar to that for POI No. 1 (Table 4 and Fig. 13). Additionally, the results of the dogboning values showed that the stents with the closed unit cells connected to themselves

(Palmaz-Schatz PS153) had large differences among the dogboning values on the POIs (11.8-43.4% for Palmaz-Schatz PS153), whereas the stents the closed unit cells connected by a bar link structure (Tenax<sup>TM</sup>) or with the opened unit cells connected by bend-shaped connector link structures (MAC Standard, MAC Q23, MAC Plus, and Coroflex) or with the opened unit cells connected by an independent straight-line link structure (RX Ultra Multi-link) had relatively small differences among the dogboning values on the POIs (4.2-29.8% for Tenax<sup>TM</sup>, 3.9-28.1% for MAC Standard, 2.4-13.2% for MAC Q23, 0.2-19.6% for MAC Plus, 7.8-32.7% for Coroflex, 7.3-23.7% for RX Ultra Multi-link) (Table 4). Here, from the magnitude of the difference, a degree of injury risk on the inner arterial wall induced by the dogboning can be expected. That is, if the difference is small, the stent is expanded evenly at the distal points of the stent, resulting in a reduction of restenosis risk.

Table 4. Summarized quantitative results of the foreshortening and dogboning behaviors of the seven commercial stents at the normal artery.

Stent	Maximum Foreshortening (%)	Maximum Dogboning (%)			
		POI No. 1	POI No. 2	POI No. 3	POI No. 4
Palmaz-Schatz PS153	6.5	53.9	37.7	25.8	10.5
Tenax <sup>TM</sup>	4.7	56.9	34.5	38.8	27.1
MAC Standard	1.5	41.4	37.5	30.1	13.3
MAC Q23	5.2	15.4	7.2	4.7	2.2
MAC Plus	1.0	31.0	31.2	24.8	11.6
Coroflex	2.4	51.9	44.0	33.0	19.2
RX Ultra Multi-link	1.5	41.3	33.9	26.6	17.6



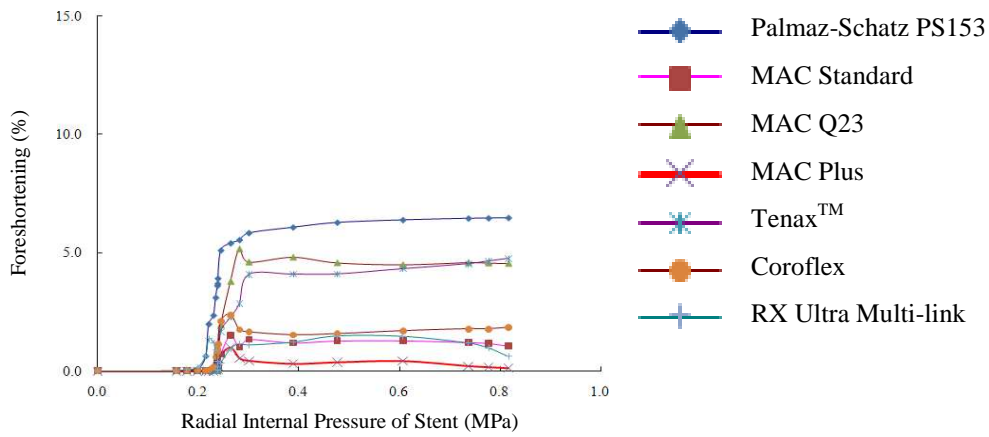


Figure 12. Forshortening (%) along with radial internal pressure (MPa) during the transient non-uniform balloon-stent expansion process obtained from the stents analyzed at the normal artery.

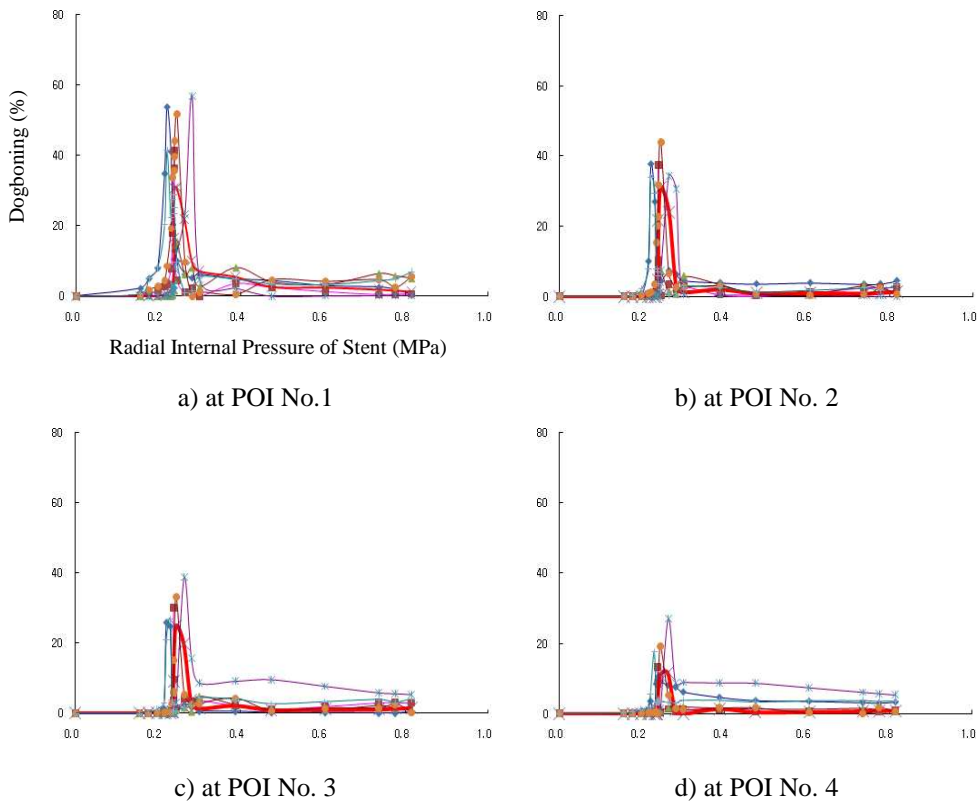


Figure 13. Dogboning (%) along with radial internal pressure (MPa) during the transient non-uniform balloon-stent expansion process obtained from the stents analyzed at the normal artery.

### C. At the 36% stenosed artery

The foreshortening and dogboning results for the seven commercial stents at the 36% stenosed artery are summarized in Table 5, and Fig. 14 and 15.

The foreshortenings, which depended on the geometrical and morphological characteristics of the stent, were ranged from 0.8% for the MAC Plus stent to 7.0% for the Palmaz-Schatz PS153 stent (Table 5 and Fig. 14). In common with results of normal artery, the foreshortening was occurred abruptly at the radial internal pressure between 0.23MPa and 0.27MPa (corresponded to regime of the second and third instant appeared during the expansion of the stent shown in Fig. 8), and was remained in an almost constant value after the radial internal pressure of 0.27MPa (corresponded to regime of the fourth instant appeared during the expansion of the stent shown in Fig. 8) for all stents (Fig. 14). Generally, the stents with the closed unit cells connected to themselves or by a bar link structure (Palmaz-Schatz PS153, Tenax<sup>TM</sup>) had higher foreshortening values, whereas the stents with the opened unit cells connected by bend-shaped connector link structures (MAC Standard, MAC Plus, and Coroflex except to MAC Q23) or by an independent straight-line link structure (RX Ultra Multi-link) had lower foreshortening values (Table 5 and Fig. 14).

The dogboning values were positive for all balloon-stents, which indicates over-expansion of the distal points (i.e., POI No.1 – POI No.4) of the stent, i.e., when the balloon-stent expanded, the distal points and the central point (POI No.5) of the stent were spread out sequentially (Table 5 and Fig. 8 and 15). The maximum dogboning value for each stent was ranged from 18.0% for the MAC Q23 stent to 52.3% for the Palmaz-Schatz PS153 stent (Table 5 and Fig. 15). For the POIs (POI No.1 – POI No.4) of all stents, the dogboning was occurred suddenly at the radial internal pressure between 0.23MPa and 0.27MPa (corresponded to regime of the second and third instant appeared during the expansion of the stent shown in Fig. 8), and was reduced and remained in an almost constant value after the radial internal pressure of 0.27MPa (corresponded to regime of the fourth instant appeared during the expansion of the stent shown in Fig. 8), similar to the foreshortening results (Fig. 15). Generally, for the POI No. 1, the stents with the closed unit cells connected to themselves (Palmaz-Schatz PS153) had higher dogboning value over 50%, whereas the stents with the closed unit cells connected by a bar link structure (Tenax<sup>TM</sup>) or with the opened unit cells connected by bend-shaped connector link structures (MAC Standard, MAC Q23, MAC Plus, and Coroflex) or by an independent straight-line link structure (RX Ultra Multi-link) had lower dogboning values below 50% (Table 5 and Fig. 15). Here, a tendency for the results of the dogboning values for other POIs was similar to that for POI No. 1 (Table 5 and Fig. 15).

Additionally, the results of the dogboning values showed that the stents with the closed unit cells connected to themselves (Palmaz-Schatz PS153) or with the opened unit cells connected by an independent straight-line link structure (RX Ultra Multi-link) had large differences among the dogboning values on the POIs (11.4-44.3% for Palmaz-Schatz PS153, 7.3-31.8% for RX Ultra Multi-link), whereas the stents the closed unit cells connected by a bar link structure (Tenax<sup>TM</sup>) or with the opened unit cells connected by bend-shaped connector link structures (MAC Standard, MAC Q23, and MAC Plus except to Coroflex) had relatively small differences among the dogboning values on the POIs (2.8-15.0% for Tenax<sup>TM</sup>, 6.0-26.4% for MAC Standard, 1.7-15.7% for MAC Q23, 1.1-20.2% for MAC Plus, 9.6-33.3% for Coroflex) (Table 5). Here, from the magnitude of the difference, a degree of injury risk on the inner arterial wall induced by the dogboning can be expected. That is, if the difference is small, the stent is expanded evenly at the distal points of the stent, resulting in a reduction of restenosis risk.

Table 5. Summarized quantitative results of the foreshortening and dogboning behaviors of the seven commercial stents at the 36% stenosed artery.

Stent	Maximum Foreshortening (%)	Maximum Dogboning (%)			
		POI No. 1	POI No. 2	POI No. 3	POI No. 4
Palmaz-Schatz PS153	7.0	52.3	37.2	25.8	8.0
Tenax <sup>TM</sup>	3.0	24.9	22.1	13.1	9.9
MAC Standard	1.0	39.8	33.8	25.0	13.4
MAC Q23	4.8	18.0	7.2	4.0	2.3
MAC Plus	0.8	30.8	29.7	23.3	10.7
Coroflex	2.3	49.9	39.0	26.3	16.6
RX Ultra Multi-link	1.4	40.9	33.6	21.0	9.1

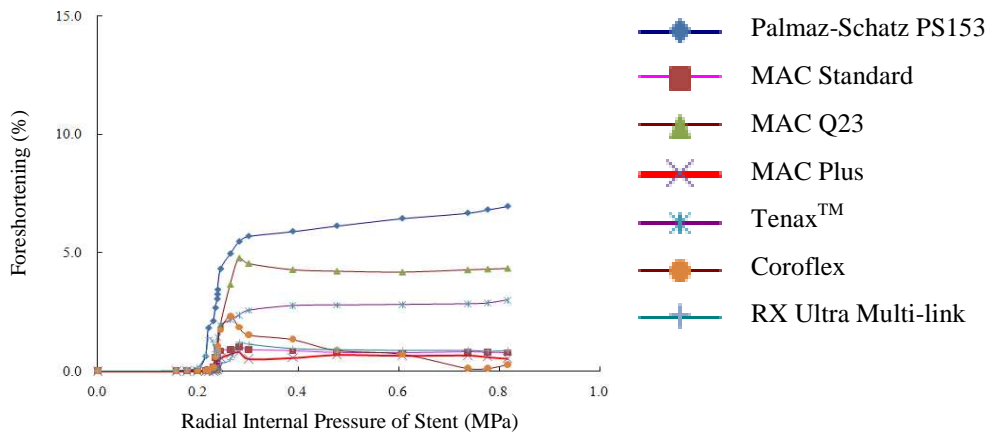


Figure 14. Forshortening (%) along with radial internal pressure (MPa) during the transient non-uniform balloon-stent expansion process obtained from the stents analyzed at the 36% stenosed artery.

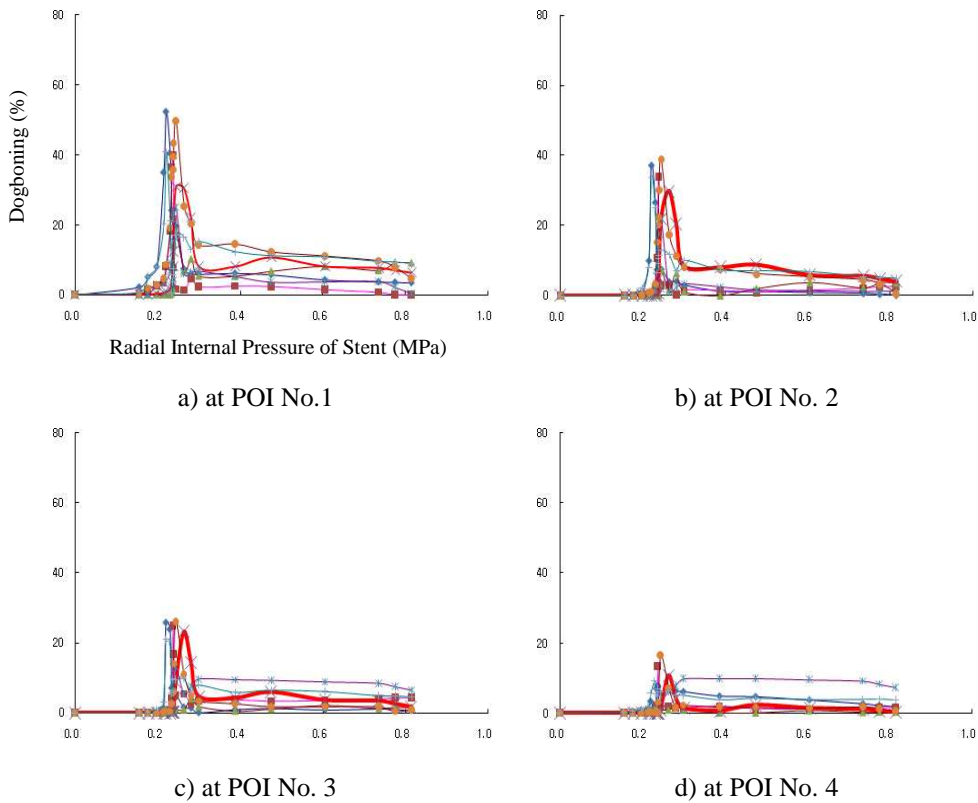


Figure 15. Dogboning (%) along with radial internal pressure (MPa) during the transient non-uniform balloon-stent expansion process obtained from the stents analyzed at the 36% stenosed artery.

#### **D. At the 64% stenosed artery**

The foreshortening and dogboning results for the seven commercial stents at the 64% stenosed artery are summarized in Table 6, and Fig. 16 and 17.

The foreshortenings, which depended on the geometrical and morphological characteristics of the stent, were ranged from 0.8% for the MAC Standard stent to 5.3% for the Palmaz-Schatz PS153 stent (Table 6 and Fig. 16). In common with results of previous simulations (at the normal artery and at the 36% stenosed artery), the foreshortening was occurred abruptly at the radial internal pressure between 0.23MPa and 0.27MPa (corresponded to regime of the second and third instant appeared during the expansion of the stent shown in Fig. 8), and was remained in an almost constant value after the radial internal pressure of 0.27MPa (corresponded to regime of the fourth instant appeared during the expansion of the stent shown in Fig. 8) for all stents (Fig. 16). Contrary to previous two results (at the normal artery and at the 36% stenosed artery), the stents with the closed unit cells connected to themselves (Palmaz-Schatz PS153) or with the opened unit cells connected by an independent straight-line link structure (RX Ultra Multi-link) had higher foreshortening values, whereas the stents with the opened unit cells connected by bend-shaped connector link structures (MAC Standard, MAC Plus, and Coroflex except to MAC Q23) or with the closed unit cells connected by a bar link structure (Tenax<sup>TM</sup>) had lower foreshortening values (Table 6 and Fig. 16).

The dogboning values were positive for all balloon-stents, which indicates over-expansion of the distal points (i.e., POI No.1 – POI No.4) of the stent, i.e., when the balloon-stent expanded, the distal points and the central point (POI No.5) of the stent were spread out sequentially (Table 6 and Fig. 8 and 17). The maximum dogboning value for each stent was ranged from 28.3% for the Tenax<sup>TM</sup> stent to 50.0% for the RX Ultra Multi-link stent (Table 6 and Fig. 17). For the POIs (POI No.1 – POI No.4) of all stents, the dogboning was occurred suddenly at the radial internal pressure between 0.23MPa and 0.27MPa (corresponded to regime of the second and third instant appeared during the expansion of the stent shown in Fig. 8), and was reduced and remained in an almost constant value after the radial internal pressure of 0.27MPa (corresponded to regime of the fourth instant appeared during the expansion of the stent shown in Fig. 8), similar to the foreshortening results (Fig. 17). Contrary to previous two results (at the normal artery and at the 36% stenosed artery), for the POI No. 1, the most of stents (Palmaz-Schatz PS153, MAC Standard, MAC Plus, Coroflex, and RX Ultra Muli-link) had higher dogboning value over 40% without reference to any morphological characteristics, whereas the stents with the closed unit cells connected by a bar link structure (Tenax<sup>TM</sup>) or

with the opened unit cells connected by bend-shaped connector link structures (MAC Q23) had lower dogboning values below 40% (Table 6 and Fig. 17). Here, a tendency for the results of the dogboning values for other POIs was similar to that for POI No. 1 (Table 6 and Fig. 17). Additionally, the results of the dogboning values showed that the stents with the closed unit cells connected to themselves (Palmaz-Schatz PS153) or with the opened unit cells connected by an independent straight-line link structure (RX Ultra Multi-link) had large differences among the dogboning values on the POIs (9.4-45.0% for Palmaz-Schatz PS153, 9.4-37.3% for RX Ultra Multi-link), whereas the stents the closed unit cells connected by a bar link structure (Tenax<sup>TM</sup>) or with the opened unit cells connected by bend-shaped connector link structures (MAC Standard, MAC Q23, and MAC Plus except to Coroflex) had relatively small differences among the dogboning values on the POIs (12.0-20.6% for Tenax<sup>TM</sup>, 11.9-21.0% for MAC Standard, 8.8-19.5% for MAC Q23, 9.1-23.4% for MAC Plus, 12.7-27.5% for Coroflex) (Table 6). Here, from the magnitude of the difference, a degree of injury risk on the inner arterial wall induced by the dogboning can be expected. That is, if the difference is small, the stent is expanded evenly at the distal points of the stent, resulting in a reduction of restenosis risk.

Table 6. Summarized quantitative results of the foreshortening and dogboning behaviors of the seven commercial stents at the 64% stenosed artery.

Stent	Maximum Foreshortening (%)	Maximum Dogboning (%)			
		POI No. 1	POI No. 2	POI No. 3	POI No. 4
Palmaz-Schatz PS153	5.3	49.9	34.7	25.4	4.9
Tenax <sup>TM</sup>	2.7	28.3	23.7	11.7	3.1
MAC Standard	0.8	42.7	30.9	18.9	9.9
MAC Q23	4.4	31.8	26.5	17.7	7.0
MAC Plus	2.3	40.5	34.9	25.8	11.5
Coroflex	3.2	49.9	40.7	28.1	13.2
RX Ultra Multi-link	4.3	50.0	40.7	31.0	12.7

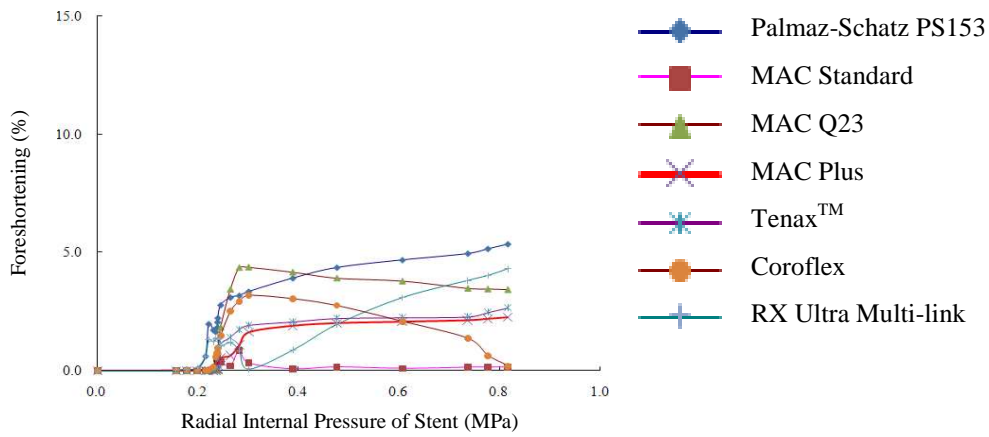


Figure 16. Forshortening (%) along with radial internal pressure (MPa) during the transient non-uniform balloon-stent expansion process obtained from the stents analyzed at the 64% stenosed artery.

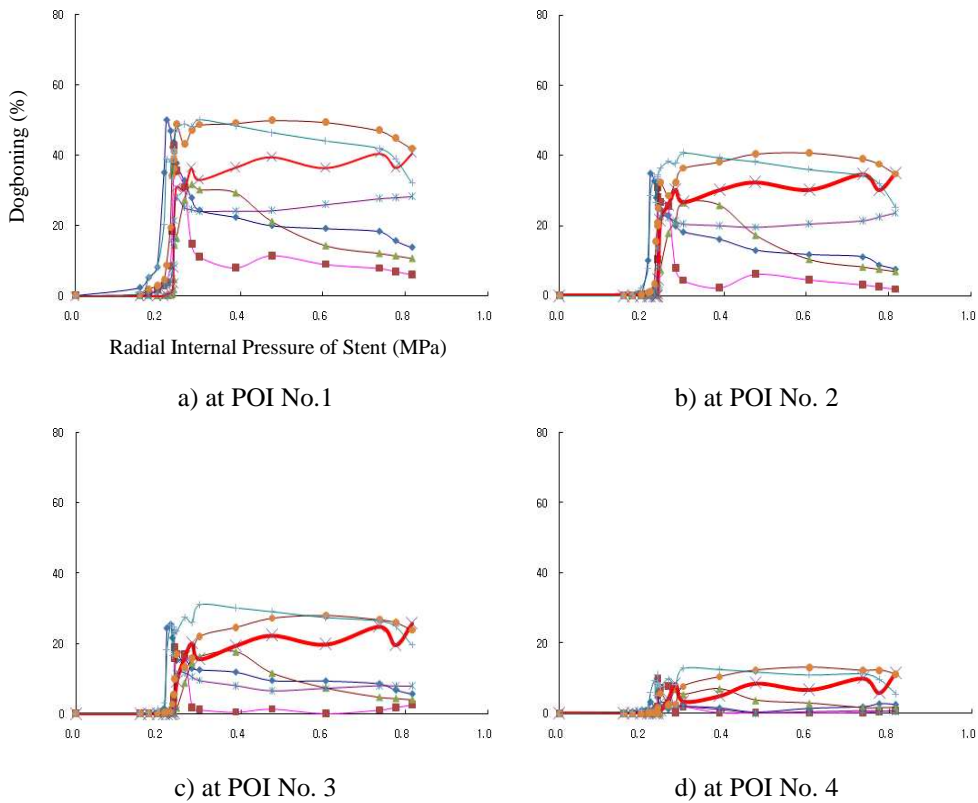


Figure 17. Dogboning (%) along with radial internal pressure (MPa) during the transient non-uniform balloon-stent expansion process obtained from the stents analyzed at the 64% stenosed artery.

### **Inner arterial wall stress of the seven commercial stents**

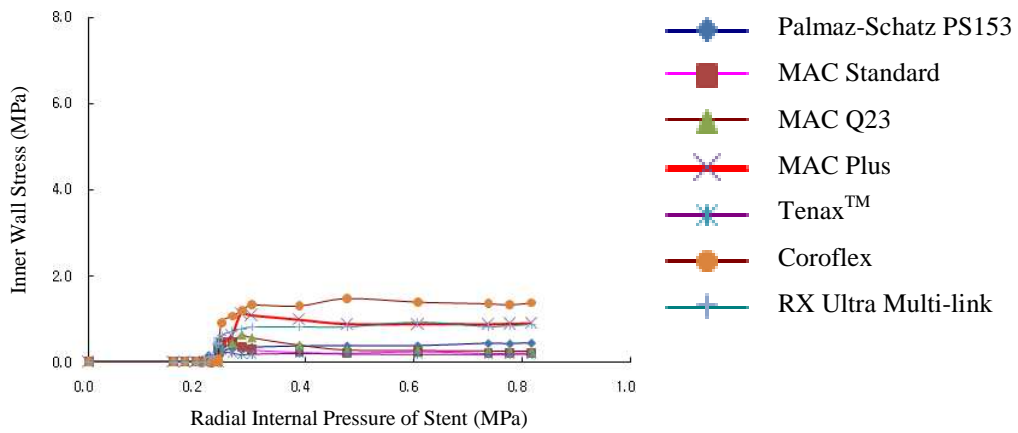
The inner arterial wall stress results for the seven commercial stents are summarized in Fig. 18.

The inner normal artery wall stresses, which depended on the geometrical and morphological characteristics of the stent, were ranged from 0.399MPa for the Tenax<sup>TM</sup> stent to 1.465MPa for the Coroflex (Fig. 18a). The inner 36% stenosed artery wall stresses were ranged from 0.632MPa for the Tenax<sup>TM</sup> stent to 6.102MPa for the Coroflex (Fig. 18b). The inner 64% stenosed artery wall stresses were ranged from 0.943MPa for the Tenax<sup>TM</sup> stent to 6.906MPa for the Coroflex (Fig. 18c).

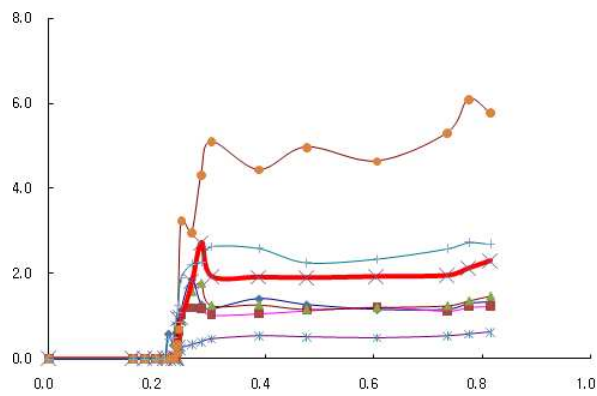
In common with results of previous simulations (foreshortening and dogboning of seven commercial stents), the maximum inner arterial wall stress was occurred abruptly at the radial internal pressure between 0.23MPa and 0.27MPa (corresponded to regime of the second and third instant appeared during the expansion of the stent shown in Fig. 8), and was remained in an almost constant value after the radial internal pressure of 0.27MPa (corresponded to regime of the fourth instant appeared during the expansion of the stent shown in Fig. 8) for all stents (Fig. 18). Contrary to previous results (foreshortening and dogboning of seven commercial stents), the stents with the opened unit cells connected by bend-shaped connector link structures (Coroflex and MAC Plus) or with the opened unit cells connected by an independent straight-line link structure (RX Ultra Multi-link) had higher inner arterial wall stress values, whereas the stents with the closed unit cells connected to themselves (Palmaz-Schatz PS153) or with the closed unit cells connected by a bar link structure (Tenax<sup>TM</sup>) had lower inner arterial wall stress values (Fig. 18).

Here, in spite of the stents with the opened unit cells connected by bend-shaped connector link structure, some stents (MAC Standard and MAC Q23) had lower inner arterial wall stress values. For this reason, besides the previous results (geometrical and morphological characteristics in connection with foreshortening and dogboning of seven commercial stents), other design parameters for decreasing of inner arterial wall stress values would be exist.

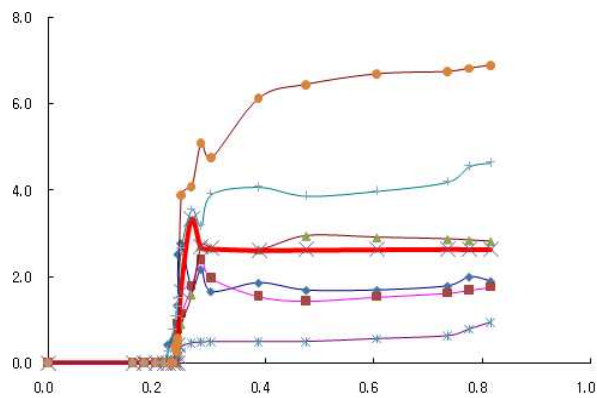




a) Normal artery



b) 36% stenosed artery



c) 64% stenosed artery

Figure 18. Inner wall stress (MPa) along with radial internal pressure (MPa) during the transient non-uniform balloon-stent expansion process obtained from the stents analyzed at the all artery.

### Aperture area of the seven commercial stents

The aperture area results for the seven commercial stents are summarized in Table 7.

The aperture areas, which depended on the geometrical and morphological characteristics of the expanded stent, were ranged from about  $1.5\text{mm}^2$  for the Tenax<sup>TM</sup> stent to  $7.1\text{mm}^2$  for the Coroflex (Table 7). In common with results of previous simulations (inner arterial wall stress of seven commercial stents), the stents with the opened unit cells connected by bend-shaped connector link structures (Coroflex and MAC Plus) or with the opened unit cells connected by an independent straight-line link structure (RX Ultra Multi-link) had higher aperture areas, whereas the stents with the closed unit cells connected to themselves (Palmaz-Schatz PS153) or with the closed unit cells connected by a bar link structure (Tenax<sup>TM</sup>) had lower aperture areas (Table 7). And also, in common with results of previous simulations (inner arterial wall stress of seven commercial stents), some stents (MAC Standard and MAC Q23) had lower aperture areas. For this reason, in case of inner arterial wall stress, it related to aperture area after stent-balloon expansion rather than geometrical and morphological characteristics of the stent. Additionally, the results of the aperture areas showed that Tenax<sup>TM</sup> ( $1.5\text{mm}^2$ ), MAC Standard ( $3.2\text{mm}^2$ ), Palmaz-Schatz PS153 ( $3.5\text{mm}^2$ ), MAC Q23 ( $3.8\text{mm}^2$ ), MAC Plus ( $4.8\text{mm}^2$ ), RX Ultra Multi-link ( $6.5\text{mm}^2$ ), Coroflex ( $7.1\text{mm}^2$ ) in ascending order (Table 7). This order was coincided with results of previous simulations (inner arterial wall stress of seven commercial stents).

Table 7. Summarized quantitative results of the aperture area of the seven commercial stents.

Stent	Areas of Inner arterial wall ( $\text{mm}^2$ )	Contact Areas of Stent ( $\text{mm}^2$ )	Average Areas per Aperture Zone ( $\text{mm}^2$ )	Relative Differences (Tenax <sup>TM</sup> based)
Palmaz-Schatz PS153	192.0	25.5	3.5	2.3
Tenax <sup>TM</sup>	153.3	20.4	1.5	1
MAC Standard	184.2	31.6	3.2	2.1
MAC Q23	178.5	26.8	3.8	2.5
MAC Plus	198.7	30.3	4.8	3.2
Coroflex	226.7	33.9	7.1	4.7
RX Ultra Multi-link	206.6	30.4	6.5	4.3

## IV. DISCUSSIONS & CONCLUSIONS

It is necessary to understand the relationship between the stent and the balloon, in order to identify an optimal stent design to minimize restenosis driven by the mechanical characteristics of stent such as foreshortening or dogboning and the intravascular injury due to high inner arterial wall stress. Carter et al.<sup>45</sup> suggested that an injury to the adjacent arterial wall during stent deployment is an important determinant of in-stent neointimal formation, and short transitional edge protection balloon technology may be useful to reduce this kind of injury. Wang et al.<sup>5</sup> also discussed an importance of transient expansion process of balloon on the injury to the adjacent arterial wall during stent deployment, quoting Squire's finding that the manner in which stents are implanted was a critical determinant of the degree of injury. With all these points in mind, how to weaken or avoid these undesirable clinical outcomes is a key question that must be answered to reduce intravascular injuries caused by foreshortening, dogboning or inner arterial wall stress. It is, therefore, especially important to pay attention to the design of the ends of the stent-balloon assembly with consideration of a realistic transient non-uniform balloon-stent expansion. This study may prove valuable as the first FE approach to investigate the design parameters capable of reducing restenosis induced by foreshortening, dogboning or inner arterial wall stress by considering a realistic transient non-uniform balloon-stent expansion.

There are basically two approaches that can be used to develop an optimal stent design by evaluating the mechanical properties of various stents. The first approach involves directly measuring the mechanical properties of the stents by taking various balloon-stent configurations and expanding them to various diameters in normal or simulated stenosed arteries, each with different characteristics. Due to the high cost, special construction, minute dimensions, dynamic characteristics of the deformation, and required animal tests, such a study would be prohibitively expensive and unachievable. The second approach involves computer analyses employing the FE method. In this way, simulations of various stents under different conditions can be carried out, and the results can be verified with experimental measurements of the specific stent behaviors. Adopting this approach reduces the costs substantially, thereby making a comparative study a viable proposition. Our FE simulations, particularly those of the transient non-uniform balloon-stent expansion, were validated favorably through comparison with experiment results reported in the literature and may be valuable for developing an optimal stent design while considering various balloon-stents configurations and different mechanical and physiological conditions.

Generally, the validation of FE models and simulations has been based on standard checks of the FE method, which should give a smooth load development, similar stress-strain plots of the structure against material property data, and smooth continuous contour lines across element boundaries. The FE models and simulations developed in the current study were validated integrally and practically by using these simple approaches as well as by comparing with experimental results from the literature. This may translate into more reasonable results for current and further applications of these FE models when studying an optimal stent design. An appropriate model of the arterial vessel and the atherosclerotic plaque, as well as correctly simulating their contact with the stent, is required to obtain fully accurate results for the mechanical behavior analysis and the optimal design of a stent. The lacks of inclusions of the blood vessel wall's mechanical characteristics such as compliance of the inner arterial wall may create significant limitations in previous study. In the previous studies, FE models have focused on stent design parameters and not on restenosis.<sup>2, 5, 10, 24, 27, 29, 31, 32, 39</sup> These studies, therefore, ignored the interaction between the stent and the inner arterial wall. However, Rogers et al.<sup>28</sup> and Prendergast et al.<sup>46</sup> presented that considering the mechanical characteristics of the inner arterial wall in FE analysis is important because the interaction may influence a function of the stent. This fact indicates that considering the mechanical characteristics of inner arterial wall may be significant for the evaluations and the design analysis of the stents. The importance of the consideration of the mechanical characteristics of the inner arterial wall is, therefore, recently increased gradually in the evaluations and the design analysis of the stents.<sup>30, 33, 47</sup> Holzapfel et al.<sup>47</sup> presented the stent and stenosed artery FE models and analyzed stress states of the investigated artery during balloon-stent expansion. Berry et al.<sup>30</sup> used the FE analysis with the stent and artery FE models to understand better how the stent structure influences the stent-implanted artery compliance and the circumferential stress at diastolic pressure. Chua et al.<sup>33</sup> performed FE simulation of the slotted tube stent with the presence of plaque and artery by balloon expansion to investigate the expansion characteristics of the slotted tube stent. However, these studies did not analyze stent design parameters (i.e., foreshortening, dogboning or inner arterial wall stress) considering the actual transient non-uniform balloon-stent expansion to be simulated necessarily for investigation of the stent design parameters related to a primary cause of restenosis. They usually considered a uniform radial internal pressure with assumption based on the fact that stent is almost uniformly dilated and finally evenly expanded. The assumption is, however, only true away from the ends of stent and at the final stage of the stent expansion process, resulting in an inaccuracy in their results because the foreshortening or the dogboning

is generally triggered at the early or middle stage of the stent expansion process as shown in Fig. 10 to 17. Although the current study addressed not only the free transient non-uniform balloon-stent expansion but also with modeling the artery, our FE models and simulations were reasonable, at least qualitatively, when compared with experimental results identified from the literature, especially since this study focused on the potential design parameters capable of reducing restenosis driven by foreshortening or dogboning through identifying these characteristics in seven commercial stents. This study may, therefore, prove valuable as the first FE approach to investigate the design parameters capable of reducing restenosis induced by the mechanical characteristics of stent such as foreshortening or dogboning and the intravascular injury due to high inner arterial wall stress by considering the realistic transient non-uniform balloon-stent expansion as mentioned above.

The foreshortening or the dogboning is generally triggered as dilating the stent by inflating the balloon. Then, the foreshortening of the stent may induce an unfavorable shearing between the stent and the artery by an abrupt contraction (shortening) in length of the stent, and the dogboning may generate an unfavorable penetration into the inner arterial wall by a sudden dilation at the edges relative to the central point of the stent (flaring of stent ends). These unfavorable shearing or penetration can make successively an injury on the inner arterial wall, resulting in restenosis of the artery. Our results showed that the foreshortening and the dogboning were triggered suddenly as the stent had the radial internal pressure between 0.23MPa and 0.27MPa in the dilation process (Fig. 10 to 17). These findings may favorably support the occurrence mechanism of the foreshortening and the dogboning of the stent, which may be generated by an abrupt contraction in the length of the stent and by a sudden dilation at the edges of the stent, respectively, as described above. Additionally, the results presenting the differences among the dogboning values on the POIs of the stents may be helpful to prediction of a degree of injury risk on the inner arterial wall, which may be induced by the dogboning of the stent. For example, if the difference is small, it indicates that a degree of injury risk on the inner arterial wall induced by the dogboning may be low because the stent is expanded evenly at the distal points of the stent although the dogboning values at the distal points are larger. Based on the fact, our results indicated that the stents with the opened unit cells connected by bend-shaped connector link structures, in particular the MAC Plus stent and MAC Standard stent, may prevent effectively restenosis caused by the dogboning.

The whole results for all stents analyzed in the current study showed that foreshortening and dogboning were generally higher in stents with closed unit cells connected by straight-line,

and were generally lower in stents with opened unit cells connected by bend-shaped link structures, in particular the MAC Plus and MAC Standard. This finding indicates that using a stent composed of opened unit cells connected by bend-shaped link structures may prevent restenosis caused by foreshortening or dogboning. And then Inner arterial wall stress results showed that stents with closed unit cells were generally lower than stents with opened unit cells, in particular the Palmaz-Schatz PS153 and Tenax<sup>TM</sup>. However, in spite of the stents with the opened unit cells connected by bend-shaped connector link structure, MAC Standard and MAC Q23 had lower inner arterial wall stress values. There (Palmaz-Schatz PS153, Tenax<sup>TM</sup>, MAC Standard and MAC Q23) had small aperture areas after expansion in common. This finding is supported by Wang et al.<sup>5</sup> and Migliavacca et al.<sup>10</sup>, Wang et al.<sup>5</sup> reported that broadening the strut of the unit cells in the distal part of the stent may decrease dogboning, and the configuration of the link structure connecting the unit cells of the stent may determine the foreshortening characteristics of the stent. Wang et al.<sup>5</sup> also found that the absence of dogboning can decrease the foreshortening of the stent to a certain extent, but this effect is limited. Migliavacca et al.<sup>10</sup> investigated the influence of the geometry of the stent on dogboning, foreshortening, and longitudinal recoiling by using FE methods and found that the thickness of the stent influenced its performance. By combining the current study with the findings of Wang et al.<sup>5</sup> and Migliavacca et al.<sup>10</sup>, we found that foreshortening, dogboning and inner arterial wall stress of stent-balloon systems were closely correlated with the configurations of the unit cells and the link structures as well as the distal geometry and morphology of the stent. Foreshortening, dogboning and inner arterial wall stress of the stent could be weakened both by using a stent composed of opened unit cells connected by the bend-shaped link structures and by controlling the distal stent strut width and thickness and by considering the aperture areas after expansion; the combination of these three methods will decrease the amount of foreshortening, dogboning and inner arterial wall stress.

Although this study provides a first look at the transient non-uniform balloon-stent expansion, there are the following limitations:

- 1) No consideration of the blood flow characteristics, and
- 2) Imperfect agreement between the stents used in the current study and in the literature<sup>5, 29, 24</sup> for validation.

This discrepancy was due to difficulties in obtaining the identical stents, balloons, and catheters that were used in the literature. However, the types of stents selected from the literature for the validation were similar to those used in the current study. These limitations will be resolved and discussed in our ongoing studies incorporated with clinical tests.

## REFERENCES

- <sup>1</sup>Timmins, L.H., et al. Stented artery biomechanics and device design optimization. *Medical and Biological Engineering and Computing*, 45:505-513, 2007.
- <sup>2</sup>Chua, S.N.D., et al. Finite element simulation of stent and balloon interaction. *Journal of Materials Processing Technology*, 143-144:591-597, 2003.
- <sup>3</sup>Fischman, D.L., et al. A randomized comparison of coronary-stent placement and balloon angioplasty in the treatment of coronary artery disease. *New England Journal of Medicine*, 331:496-501, 1994.
- <sup>4</sup>Serruys, P.W., et al. A comparison of balloon-expandable stent implantation with balloon angioplasty in patients with coronary artery disease. *New England Journal of Medicine*, 331:489-495, 1994.
- <sup>5</sup>Wang, W.Q., et al. Analysis of the transient expansion behavior and design optimization of coronary stents by finite element method. *Journal of Biomechanics*, 39:21-32, 2006.
- <sup>6</sup>Kandzari, D.E., et al. Coronary artery stents: Evaluating new designs for contemporary percutaneous intervention. *Catheterization and Cardiovascular Interventions*, 56:562-576, 2002.
- <sup>7</sup>Suwaidi, A.I., et al. Coronary artery stents. *Journal of the American Medical Association*, 284:1828-1836, 2000.
- <sup>8</sup>Dotter, C.T. Transluminally placed coil spring end arterial tube graft, long-term patency in canine popliteal artery. *Investigative Radiology*, 4:329-332, 1969.
- <sup>9</sup>Dangas, G. and V. Fuster. Management of restenosis after coronary intervention. *American Heart Journal*, 132:428-436, 1996.
- <sup>10</sup>Migliavacca, F., et al. Mechanical behavior of coronary stents investigated through the finite element method. *Journal of Biomechanics*, 35:803-811, 2002.
- <sup>11</sup>Erbel, R., et al. Coronary-artery stenting compared with balloon angioplasty for restenosis after initial balloon angioplasty. *New England Journal of Medicine*, 339:1672-1678, 1998.
- <sup>12</sup>Freitag, L., et al. Theoretical and experimental basis for development of dynamic airway stent. *European Respiratory Journal* 7:2038-2045, 1994.
- <sup>13</sup>Wong, P., et al. Migration of the AVE micro coronary stent. *Catheterization and Cardiovascular Diagnosis*, 38:267-27, 1996.
- <sup>14</sup>Bjarnason, H., et al. Collapse of a Palmaz stent in the subclavian vein *American Journal of Roentgenology*, 160:1123-1124, 1993.
- <sup>15</sup>Rosenfield, K., et al. Restenosis of endovascular stents from stent compression. *Journal of American College of Cardiology*, 29:328-338, 1997.
- <sup>16</sup>Lohavanichbutr, K., et al. Mechanisms, management, and outcome of failure of delivery of coronary stents. *American Journal of Cardiology*, 83:779-781, 1999.

- <sup>17</sup> Stefanidis, I.K., et al. Development in intracoronary stents. *Hellenic Journal Cardiology*, 43:63-67, 2002.
- <sup>18</sup> Kastrati, A., et al. Restenosis after coronary placement of various stent types. *American Journal of Cardiology*, 87:34-39, 2001.
- <sup>19</sup> Schwartz, R.S. Pathophysiology of restenosis: Interaction of thrombosis, hyperplasia, and/or remodeling. *The American Journal of Cardiology*, 81:14E-17E, 1998.
- <sup>20</sup> Karas, S., et al. Coronary intimal proliferation after balloon injury and stenting in swine: an animal model of restenosis. *Journal of the American College of Cardiology*, 20:467-474, 1992.
- <sup>21</sup> den Heijer, et al. Angioscopic versus angiographic detection of intimal dissection and intracoronary thrombus. *Journal of the American College of Cardiology*, 24:649-654, 1994.
- <sup>22</sup> Wilensky, R., et al. Vascular injury, repair, and restenosis after percutaneous transluminal angioplasty in the atherosclerotic rabbit. *Circulation*, 92:2995-3005, 1995.
- <sup>23</sup> Deitch, J. S., et al. Effects of beta3-integrin blockade (c7E3) on the response to angioplasty and intra-arterial stenting in atherosclerotic nonhuman primates. *Arteriosclerosis, Thrombosis, and Vascular Biology*, 18:1730-1737, 1998.
- <sup>24</sup> Migliavacca, F., et al. A predictive study of the mechanical behavior of coronary stents by computer modeling. *Medical Engineering and Physics*, 27:13-18, 2005.
- <sup>25</sup> Balossino, R., et al. Effects of different stent designs on local hemodynamics in stented arteries. *Journal of Biomechanics*. 41:1053-1061, 2008.
- <sup>26</sup> Hara, H., et al. Role of stent design and coatings on restenosis and thrombosis. *Advanced Drug Delivery Reviews*. 58:377-386, 2006.
- <sup>27</sup> Etave, F., et al. Mechanical properties of coronary stents determined by using finite element analysis *Journal of Biomechanics*, 34:1065-1075, 2001.
- <sup>28</sup> Rogers, C., et al. Balloon artery interactions during stent placement. A finite element analysis approach to pressure, compliance, and stent design as contributors to vascular injury. *Circulation Research*, 84:378-383, 1999.
- <sup>29</sup> Dumoulin, C. and B. Cochelin. Mechanical behavior modeling of balloon-expandable stents. *Journal of Biomechanics*, 33:1461-1470, 2000.
- <sup>30</sup> Berry, J.L., et al. Hemodynamics and wall mechanics of a compliance matching stent: In vitro and in vivo analysis. *Journal of Vascular Interventional and Radiology*, 13:97-105, 2002.
- <sup>31</sup> Chua, S.N.D., et al. Finite-element simulation of stent expansion. *Journal of Materials Processing Technology*, 120:335-340, 2002.
- <sup>32</sup> Chua, S.N.D., et al. Effects of varying slotted tube (stent) geometry on its expansion behaviour using finite element method. *Journal of Materials Processing Technology*, 155-156:1764-1771, 2004.



- <sup>33</sup> Chua, S.N.D., et al. Finite element simulation of slotted tube (stent) with the presence of plaque and artery by balloon expansion. *Journal of Materials Processing Technology*, 155-156:1772-1779, 2004.
- <sup>34</sup> Auricchio, F., et al. Finite-element Analysis of a Stenotic Artery Revascularization through a Stent Insertion. *Computer Methods in Biomechanics and Biomedical Engineering*, 4:249-263, 2001.
- <sup>35</sup> Lally, C., et al. Cardiovascular stent design and vessel stresses: a finite element analysis. *Journal of Biomechanics*, 38:1574-1581, 2005.
- <sup>36</sup> Walke, W., et al. Experimental and numerical biomechanical analysis of vascular stent. *Journal of Materials Processing Technology*, 164-165:1263-1268, 2005.
- <sup>37</sup> Takashima, K., et al. Simulation and experimental observation of contact conditions between stents and artery models. *Medical Engineering & Physics*, 29:326-335, 2007.
- <sup>38</sup> Gay, M., et al. Stent modeling using immersed finite element method. *Computer Methods in Applied Mechanics and Engineering*, 195:4358-4370, 2006.
- <sup>39</sup> Migliavacca, F., et al. Stainless and shape memory alloy coronary stents: A computational study on the interaction with the vascular wall *Biomechanics and Modeling in Mechanobiology*, 2:205-217, 2004.
- <sup>40</sup> Migliavacca, F., et al. A predictive study of the mechanical behaviour of coronary stents by computer modelling. *Medical Engineering and Physics*, 27:13-18, 2004.
- <sup>41</sup> Albertini, C. and M. Montagnani. Dynamic uniaxial and biaxial stress-strain relationships for austenitic stainless steels. *Nuclear Engineering and Design*, 57:107-123, 1980.
- <sup>42</sup> MatWeb. Dupont Fusabond E MB100D High Density Polyethylene, Available at <http://www.matweb.com/search/SpecificMaterial.asp?bassnum=PDUPM015>. MatWeb Material Property Data, 2006.
- <sup>43</sup> Lally, C., et al. An investigation into the applicability of a Mooney–Rivlin constitutive equation for modeling vascular tissue in cardiovascular stenting procedures. *Proceedings of the International Congress on Computational Biomechanics*, Zaragoza, Spain, 542–550, 2003.
- <sup>44</sup> Wang, W.Q., et al. Analysis of the transient expansion behavior and design optimization of coronary stents by finite element method. *Journal of Biomechanics*, 39:21-32, 2006.
- <sup>45</sup> Carter, A.J., et al. Experimental evaluation of a short transitional edge protection balloon for intracoronary stent deployment. *Catheterization and Cardiovascular Interventions*, 51:112-119, 2000.
- <sup>46</sup> Prendergast, P.J., et al. Analysis of prolapse in cardiovascular stents: A constitutive equation for vascular tissue and finite-element modelling. *Journal of Biomechanical Engineering* 125:692-699, 2003.
- <sup>47</sup> Holzapfel, G., et al. A Layer-Specific Three-Dimensional Model for the Simulation of Balloon Angioplasty using Magnetic Resonance Imaging and Mechanical Testing. *Annals of Biomedical Engineering*, 30:753-767, 2002.

## 국문요약

### 혈관용 스텐트의 비정상적인 혈관 내 팽창을 고려한 재협착을 감소시키는 설계요소에 대한 연구

< 지도교수: 김 한 성 >

연세대학교 일반대학원 의공학과

박 원 필

혈관용 스텐트의 비정상적인 혈관 내 거동으로 인해 발생하는 길이방향단축현상(Fore-shortening)과 도그보닝(Dogboning)은 혈관 내부에 상해를 발생시키고, 이는 결과적으로 재협착으로 발전한다. 이전의 연구들은 혈관용 스텐트의 기계적 특성과 혈관 내 이식되는 스텐트의 거동을 분석함에 있어서 혈관용 스텐트의 비정상적인 혈관 내 거동의 영향을 고려하지 않았고, 길이방향단축현상과 도그보닝에 의해 야기되는 재협착의 발생을 감소시키는 설계요소와 혈관 내벽에 응력 값을 감소시키는 설계요소에 대한 연구도 미비한 실정이다. 따라서 본 연구에서는 7 개의 상용화된 혈관용 스텐트들에 대해서 비정상적인 혈관 내 거동을 고려한 유한요소해석을 수행하여 길이방향단축현상과 도그보닝에 의해 야기되는 재협착의 발생을 감소시키는 설계요소와 혈관 내벽에 응력 값을 감소시키는 설계요소에 대해 연구하였다. 연구 결과, 곡선 형태의 링크로 연결된 개방형 유닛 셀 구조의 스텐트와 스텐트의 양 끝단에 위치한 유닛 셀과 링크구조의 기하학적이고 형태학적인 특징들을 조절함으로써 길이방향단축현상과 도그보닝에 의해 야기되는 재협착의 발생을 감소시킬 수 있을 것이다. 또한 곡선 형태의 링크로 연결된 개방형 유닛 셀 구조의 스텐트가 확장된 후, 혈관 내벽의 공극을 최소화시키는 유닛 셀과 링크구조의 기하학적이고 형태학적인 특징들을 조절함으로써 혈관 내벽의 응력 값을 감소시킬 수 있을 것이다. 본 연구는 이전 연구들보다 더 사실적인 스텐트의 비정상적인 혈관 내 팽창을 고려함으로써 재협착의 발생을 감소시키는 혈관용 스텐트의 설계요소에 대해 연구하였다는데 그 의의가 있다.

---

**핵심되는 말** : 혈관용 스텐트, 길이방향단축현상, 도그보닝, 비정상적인 풍선팽창, 유한요소해석

## Author's Accomplishment

### International Journal (SCI)

1. Dohyung Lim, **Won-Pil Park**, Qyoun-Jung Lee, Han-Sung Kim, Yong-Heum Lee, "Development and Clinical Testing of an Ultrasonic Diagnostic System for Functional Gastrointestinal Disorders," *Ultrasound in Medicine and Biology*, Vol. 34, No. 6, pp.874-884, 2008.
2. Dohyung Lim, Dae-Gon Woo, **Won-Pil Park**, Yong-Heum Lee, Han-Sung Kim, In-Deok Kong, "Alterations to the Mechanical Response of the Gastrointestinal Tract Induced by Functional Gastrointestinal Disorders and the Feasibility of Developing an Ultrasonic Diagnostic System," *Journal of Mechanical Science And Technology*, Vol. 22, pp.846-855, 2008.
3. Dohyung Lim, Seung-Kwan Cho, **Won-Pil Park**, Anders Kristensson, Jai-Young Ko, S.T.S. Al-Hassani, Han-Sung Kim, "Suggestion of Potential Stent Design Parameters to Reduce Restenosis Risk driven by Foreshortening or Dogboning due to Non-uniform Balloon-Stent Expansion," *Annals of Biomedical Engineering*, Vol. 36, No. 7, pp.1118-1129, 2008.
4. Seung-Hwan Youn, Seong-Ho Choi, Kyoo-Sung Cho, Jung-Kiu Chai, Chong-Kwan Kim, **Won-Pil Park**, Dohyung Lim, Han-Sung Kim, "Three-Dimensional Finite Element Analysis of Stability in Proportion to Crown-to-Implant Ratio in the Implant-supported Prostheses," *The International Journal of Oral and Maxillofacial Implants*, Revising.

### International Journal (Non-SCI)

1. **Won-Pil Park**, Qyoun-Jung Lee, Dae-Gon Woo, Chang-Yong Ko, Eun-Geun Kim, Dohyung Lim, Yong-Heum Lee, Tae-Min Shin, and Han-Sung Kim, "Suggestion of Ultrasonic System for Diagnosis of Functional Gastrointestinal Disorders Finite Difference Analysis, Development and Clinical Trials," *International Journal of Biomedical Sciences*, Vol. 1, No. 1, pp.200-206, 2006.
2. **Won-Pil Park**, Seung-Kwan Cho, Jai-Young Ko, Anders Kristensson, S.T.S. Al-Hassani, Han-Sung Kim, and Dohyung Lim, "Evaluation of Stent Performances using FEA considering a Realistic Balloon Expansion," *International Journal of Mathematical, Physical and Engineering Sciences*, Vol. 2, No. 2, pp.103-108, 2008.
3. Eun-Geun Kim, **Won-Pil Park**, Dae-Gon Woo, Chang-Yong Ko, Yong-Heum Lee, Dohyung Lim, Tae-Min Shin, Han-Sung Kim, and Gyoung-Jung Lee, "Ultrasonic System for Diagnosis of Functional Gastro-intestinal Disorders : Development, Verification and Clinical Trials," *International Journal of Biomedical Sciences*, Vol. 1, No. 1, pp.207-212, 2006.

### Domestic Journal

1. **박원필**, 우대곤, 고창용, 이균정, 이용흠, 최서형, 신태민, 김한성, 임도형, "유한차분법을 이용한 기능성 위장 장애 진단용 초음파 시스템의 개발," *한국정밀공학회지*, Vol. 24, No. 9, pp.130-139, 2007.
2. 임도형, 김은근, 이균정, **박원필**, 김한성, 신태민, 최서형, 이용흠, "초음파 응답특성 분석에 의한 위장 경화 진단시스템의 설계," *대한의공학회지*, Vol. 28, No. 2, pp.250-257, 2007.

### International Conference

1. **Won-Pil Park**, Qyoun-Jung Lee, Dae-Gon Woo, Chang-Yong Ko, Eun-Geun Kim, Dohyung Lim, Yong-Heum Lee, Tae-Min Shin, Han-Sung Kim, "Suggestion of Ultrasonic System for Diagnosis of Functional Gastrointestinal Disorders: Finite Difference Analysis, Development and Clinical Trials, " *International Conference on Computer & Information Science and Engineering 2007*, Vol. 19, pp.258-264, 2007.
2. **Won-Pil Park**, Dohyung Lim, Seung-Kwan Cho, Anders Kristensson, S.T.S. Al-Hassani, Jai-Young Ko and Han-Sung Kim, "Design Parameters to Reduce a Possibility of Restenosis: Finite Element Analysis," *Asian Symposium for Precision Engineering and Nanotechnology 2007*, pp.416-418, 2007.
3. **Won-Pil Park**, Dohyung Lim, Seung-Hwan Youn and Han-Sung Kim, "Evaluation of Stability in Proportion to Crown - Implant Ratio using Finite Element Analysis," *Asian Symposium for Precision Engineering and Nanotechnology 2007*, pp.419-421, 2007.
4. **Won-Pil Park**, Seung-Kwan Cho, Jai-Young Ko, Anders Kristensson, S.T.S. Al-Hassani, Han-Sung Kim, and Dohyung Lim, "Evaluation of Stent Performances using FEA considering a Realistic Balloon Expansion, " *International Conference on Computer, Electrical, and Systems Science, and Engineering*, pp.117-122, 2008.
5. Eun-Geun Kim, **Won-Pil Park**, Dae-Gon Woo, Chang-Yong Ko, Yong-Heum Lee, Dohyung Lim, Tae-Min Shin, Han-Sung Kim, Gyoung-Jung Lee, "Ultrasonic System for Diagnosis of Functional Gastrointestinal Disorders: Development, Verification and Clinical Trials," *International Conference on Computer & Information Science and Engineering 2007*, Vol. 19, pp.265-270, 2007.
6. Qyoun-Jung Lee, **Won-Pil Park**, Dohyung Lim, Dae-Gon Woo, Chang-Yong Ko, Dong-Ha Lee, Yong-Heum Lee, Han-Sung Kim, Hyoung-Ro Yoon, Tae-Min Shin, "Ultrasonic System for Diagnosis of Functional Gastrointestinal Disorders: Development, Verification and Clinical Trials," *The 2nd Frontier in Biomedical Devices Conference*, pp.38080, 2007.
7. Seung-Kwan Cho, **Won-Pil Park**, Eun-Jung Cho, Dohyung Lim, Han-Sung Kim and Jai-Young Ko, "Comparative Studies of Different Vascular Stents in terms of Mechanical

- Performances: Finite Element Analysis," *The 4th Latin American Congress on Biomedical Engineering*, Vol. 18, pp.744-747, 2007.
8. Young-Kuen Cho, **Won-Pil Park**, Chang-Yong Ko, Seung-Hwan Youn, Dohyung Lim and, Han-Sung Kim, "Stability Evaluation in Terms of Crown to Fixture Ratio of Dental Implant: Finite Element Analysis," *The 3rd Asian Pacific Conference on Biomechanics*, pp.s222, 2007.
  9. Dae Gon Woo, Dohyung Lim, **Won-Pil Park**, Dong Jin Seo, In Deok Kong and Han Sung Kim, "Alteration of Mechanical Characteristic on the Gastrointestinal Tract with Functional Gastrointestinal Disorders," *The 21th Congress of International Society of Biomechanics*, Vol. 40, Suppl. 2, pp.s679, 2007.
  10. Seung-Kwan Cho, Han-Sung Kim, Young-Ho Kim, **Won-Pil Park**, Mohsen Makhsoos, Dohyung Lim, "Evaluation of Interface Pressure and Internal Stress Relief Effects Achieved by Functional Electrical Stimulation: Finite Element Analysis," *The 2nd International Conference on Advanced Nondestructive Evaluation*, pp.117, 2007.

#### Domestic Conference

1. **박원필**, 조승관, 조은정, 김한성, 고재영, "전산모의해석을 이용한 스텐트의 기계적 특성에 관한 연구," *2006년도 한국정밀공학회 추계학술대회 논문집*, pp.563-564, 2006.
2. **박원필**, 조승관, 조은정, 임도형, 고재영, 김민수, 김한성, "반응표면법을 이용한 혈관용 스텐트의 설계," *2007년도 한국정밀공학회 생체공학부문 학술대회 논문집*, Vol. 1, pp.141-143, 2007.
3. 임도형, 조승관, **박원필**, 손량희, 김영호, 김한성, "유한요소법을 이용한 무릎 보조기 착용에 따른 영향 평가," *2008년도 한국정밀공학회 춘계학술대회 논문집*, pp.257-258, 2008.
4. 전창수, 강성찬, 윤유경, **박원필**, 정영준, 장광희, 김한성, 심준성, "유한요소해석을 이용한 한국인(여성) 치아의 형상에 따른 표준화 연구," *2005년도 대한의용생체공학회 춘계학술대회 논문집*, pp.436-439, 2005.

#### Award

1. 2006년 추계학술대회 우수논문발표 장려상, 한국정밀공학회, 2006년 11월 17일.

#### Patent

1. 출원일자 : 2007.11.01, 출원번호 : 10-2007-0111064